1-1-2017

Post-Rift Magmatic Evolution of the Eastern North American “Passive-Aggressive” Margin

Sarah E. Mazza
Virginia Polytechnic Institute and State University, smazza@smith.edu

Esteban Gazel
Virginia Polytechnic Institute and State University

Elizabeth A. Johnson
James Madison University

Michael Bizimis
University of South Carolina

Ryan McAleer
United States Geological Survey

See next page for additional authors

AGU PUBLICATIONS

Geochemistry, Geophysics, Geosystems

RESEARCH ARTICLE
10.1002/2016GC006646

Post-rift magmatic evolution of the eastern North American "passive-aggressive" margin

Sarah E. Mazza[1], Esteban Gazel[1], Elizabeth A. Johnson[2], Michael Bizimis[3], Ryan McAleer[4], and C. Berk Biryol[5]

[1]Department of Geosciences, Virginia Tech, Blacksburg, Virginia, USA, [2]Department of Geology and Environmental Science, James Madison University, Harrisonburg, Virginia, USA, [3]Department of Earth and Ocean Sciences, University of South Carolina, Columbia, South Carolina, USA, [4]United States Geological Survey, Reston, South Carolina, USA, [5]Department of Geological Sciences, University of North Carolina at Chapel Hill, Chapel Hill, North Carolina, USA

Key Points:
- Bimodal late Jurassic volcanics in Virginia-West Virginia produced by tectonic instabilities remnant of the rifting of Pangea
- The Eastern North American passive margin is characterized by pulses of postrift alkaline magmatic activity up to 150 Ma following rifting
- Pulses of magmatism and rejuvenation events in Eastern North American margin fail to fit the traditional passive-margin definition

Supporting Information:
- Supporting Information S1
- Figure S1
- Figure S2
- Figure S3
- Figure S4
- Figure S5
- Figure S6
- Figure S7
- Table S1
- Table S2
- Table S3

Correspondence to:
E. Gazel,
egazel@vt.edu

Citation:
Mazza, S. E., E. Gazel, E. A. Johnson, M. Bizimis, R. McAleer, and C. B. Biryol (2017), Post-rift magmatic evolution of the eastern North American "passive-aggressive" margin, *Geochem. Geophys. Geosyst.*, *18*, 3–22, doi:10.1002/2016GC006646.

Received 15 SEP 2016
Accepted 22 NOV 2016
Accepted article online 26 NOV 2016
Published online 9 JAN 2017

Abstract Understanding the evolution of passive margins requires knowledge of temporal and chemical constraints on magmatism following the transition from supercontinent to rifting, to post-rifting evolution. The Eastern North American Margin (ENAM) is an ideal study location as several magmatic pulses occurred in the 200 My following rifting. In particular, the Virginia-West Virginia region of the ENAM has experienced two postrift magmatic pulses at ~152 Ma and 47 Ma, and thus provides a unique opportunity to study the long-term magmatic evolution of passive margins. Here we present a comprehensive set of geochemical data that includes new $^{40}Ar/^{39}Ar$ ages, major and trace-element compositions, and analysis of radiogenic isotopes to further constrain their magmatic history. The Late Jurassic volcanics are bimodal, from basanites to phonolites, while the Eocene volcanics range from picrobasalt to rhyolite. Modeling suggests that the felsic volcanics from both the Late Jurassic and Eocene events are consistent with fractional crystallization. Sr-Nd-Pb systematics for the Late Jurassic event suggests HIMU and EMII components in the magma source that we interpret as upper mantle components rather than crustal interaction. Lithospheric delamination is the best hypothesis for magmatism in Virginia/West Virginia, due to tectonic instabilities that are remnant from the long-term evolution of this margin, resulting in a "passive-aggressive" margin that records multiple magmatic events long after rifting ended.

1. Introduction

The Eastern North American Margin (ENAM) has been interpreted as a passive margin that developed after the rifting of Pangea and the subsequent opening of the Atlantic Ocean basin approximately 200 Mya [e.g., *Faill*, 1998; *Bradley*, 2008]. However, the ENAM has experienced tectonic rejuvenation post-rifting evident by topographic rejuvenation, ongoing seismic activity, and pulses of magmatic activity. Topographic rejuvenation is marked by increased erosion rates and unsteady sediment deposition [*Pazzaglia and Brandon*, 1996; *McKeon et al*., 2014], and drainage reorganization [*Miller et al*., 2013; *Prince and Spotila*, 2013] which have been linked to mantle-driven dynamic topography [*Rowley et al*., 2013]. The 2011 Mineral, Virginia earthquake (M5.8) [*Horton et al*., 2015] in the Central Virginia Seismic Zone and the 1886 Charleston, South Carolina earthquake (M6.9) [*Bakun and Hopper*, 2004] in the Charleston Seismic Zone are just two examples of strong earthquakes in the recent seismic record in the ENAM. Postrift magmatism from the late Jurassic (152 Ma) [*Johnson et al*., 1971] to Eocene (47 Ma) [*Johnson et al*., 1971; *Southworth et al*., 1993; *Mazza et al*., 2014] is preserved from Virginia to Quebec [*Eby*, 1984, 1985; *Foland et al*., 1986]. These indicators of tectonic rejuvenation highlight the not-so-passive nature of the ENAM and suggest that passive margins are not as geologically stable as conventionally thought.

Incipient rift systems like the Red Sea-Gulf of Aden-East Africa rift system are useful for understanding the early development of passive margins [*Sahota et al*., 1995; *Izzeldin*, 1987; *Pallister et al*., 2010; *Korostelev et al*., 2016; *Ebinger et al*., 2010]. Yet, in order to understand the full evolution of passive margins, we need to include areas that have been evolving for 10's of millions of years, such as ENAM. The ENAM is an ideal region to study the evolution of passive margins, and geochemical analysis of multiple magmatic events scattered throughout the ENAM can help to improve our knowledge of the processes that affect postrift margins.

Here, we present a comprehensive set of new geochemical and geochronological data for the Late Jurassic and Eocene volcanics from the northern Valley and Ridge of Virginia and West Virginia, which includes new $^{40}Ar/^{39}Ar$ ages for the Late Jurassic magmatic pulse along with a complete whole-rock major and trace-element analysis of these alkaline volcanics, and the first Sr-Nd-Pb radiogenic isotopic data for these rocks. The Eocene samples included here are in addition to previously published samples [*Mazza et al*., 2014], with additional $^{40}Ar/^{39}Ar$ ages that confirm Eocene magmatic activity, and the first discussion of the production of cogenetic felsic magmas. This comprehensive data set will help understand Late Jurassic and Eocene magmatism and improve our understanding of processes associated with the post-rift magmatic activity in so-called passive margins.

2. Geological Background

The ENAM experienced multiple orogenic events, locally known as Grenville (~1.2–0.9 Ga), Taconic (~470–440 Ma), Acadian (~420–360 Ma), and Alleghanian (~320–260 Ma) and supercontinent breakup with Rodinia at ~570 Ma, and Pangea at ~200 Ma [*Tollo et al*., 2004; *Hatcher*, 2002, 2010]. Starting in the Mesozoic, the ENAM has also experienced multiple magmatic events, not all clearly associated with tectonic events. The rifting of Pangea at ~200 Ma is related to the widespread magmatism of the Central Atlantic Magmatic Province (CAMP) [*Nomade et al*., 2007; *Marzoli et al*., 2011; *Blackburn et al*., 2013; *Callegaro et al*., 2013; *Whalen et al*., 2015]. CAMP is preserved throughout the ENAM [*Whalen et al*., 2015] and is located near Late Jurassic and Eocene volcanics of northwest Virginia-West Virginia (Figure 1) [*Johnson et al*., 1971; *De Boer et al*, 1988; *Mazza et al*., 2014]. CAMP has been associated with a possible super plume [e.g., *Wilson*, 1997], but *Whalen et al*. [2015] proposed that the breakup of Pangea, and the formation of CAMP, is related to a massive detachment of the low angle subducting Rheic plate which existed between the modified Laurentian margin (North America) and Gondwana prior to the Alleghenian orogeny. They found that the source of CAMP was significantly modified by subduction processes and melted at temperatures below what is expected from mantle plume activity.

Pangea rifting and CAMP magmatism initiated the ENAM's development into a passive margin [*Puffer*, 2001, 2003; *Whalen et al*., 2015], but the subsequent pulses of volcanic activity, plus recent mantle-influenced, dynamic topographic increase [e.g., *Rowley et al*., 2013]. This suggests that the passive margin is in fact a dynamically active margin, meaning that even though traditional tectonic forces no longer have an effect on the margin, it is still changing due to the dynamics of the lithosphere and the mantle. Two magmatic events are recorded in the northern Valley and Ridge of Virginia-West Virginia: a Late Jurassic pulse that erupted approximately 50 My after the initiation of rifting, followed by an Eocene pulse approximately 100 My later [*Johnson et al*., 1971; *Mazza et al*., 2014].

Postrifting magmatism is not limited to Virginia-West Virginia. The ENAM experienced other Jurassic to Cretaceous magmatic events such as those recorded at the Monteregian Hills alkaline province in Quebec [*Eby*, 1984, 1985; *Foland et al*., 1986; *Roulleau et al*., 2013], the White Mountain Magma Series in New England, and the New England seamounts, all of which have been connected to the proposed Great Meteor hotspot (Figure 1) [*Crough*, 1981; *Duncan*, 1984; *McHone and Butler*, 1984; *Jansa and Pe-Piper*, 1988; *Klitgord et al*., 1988; *McHone*, 1996]. Late Jurassic-Early Cretaceous kimberlitic magmatism in New York and Pennsylvania have been associated with the Great Meteor Hotspot [*Heaman and Kjarsgaard*, 2000; *Bikerman et al*., 1997].

A series of Late Jurassic alkaline volcanics are found in the Valley and Ridge province of northern Virginia-West Virginia, alongside CAMP and Eocene volcanics [*Johnson et al*., 1971; *Southworth et al*., 1993]. K-Ar dating of a nepheline syenite from Augusta County, Virginia first constrained these alkaline units to the Late Jurassic (145 ± 7 Ma and 153 ± 8 Ma for biotite and amphibole, respectively) [*Zartman et al*., 1967]. *Johnson et al*. [1971] gave the first detailed petrology for the Augusta County alkaline suite, and a recent study by *Meyer and van Wijk* [2015] presented detailed geochemistry for these Late Jurassic alkaline lavas, but limits Late Jurassic magmatism to a ~1000 km^2 elliptical area in Augusta County. *Southworth et al*. [1993] had Late Jurassic magmatism encompass a larger region that included Pendleton County, West Virginia, with a $^{40}Ar/^{39}Ar$ date of 147.0 ± 0.7 Ma from a mica pyroxenite. *Meyer and van Wijk* [2015] proposed that Late Jurassic volcanism were produced by lithospheric delamination that resulted with the delaminated material interacting with the surrounding mantle lithosphere to trigger melting.

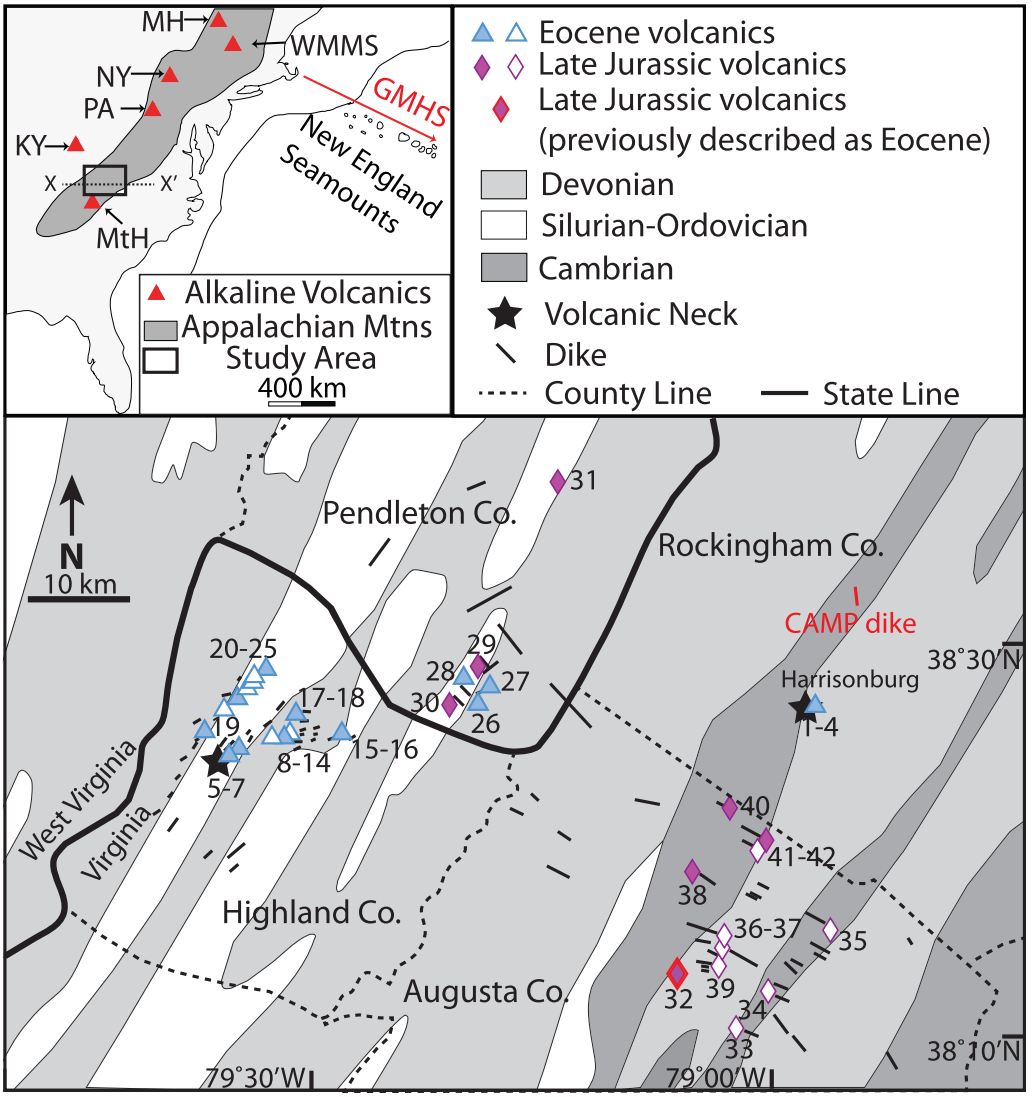

Figure 1. Simplified geological map (modified from *Dicken et al.* [2005]) showing sample locations of the Late Jurassic and Eocene volcanic rocks, with closed symbols representing samples of mafic ($SiO_2 < 50$ wt %) composition and open symbols representing samples of felsic ($SiO_2 > 50$ wt %) composition. The Late Jurassic dikes trend to the NW while the Eocene dikes trend to the NE. One NW trending dike in field area has been identified as belonging to the Central Atlantic Magmatic Province, shown in red and labeled on map [*Mazza et al.*, 2014]. GPS coordinates are provided in supporting information Table S1. Inset map shows other alkaline/kimberlitic volcanics found in the ENAM, MtH – Mount Horeb Kimberlite, Virginia, KY – Elliot County Kimberlite, Kentucky, PA – Masonville Kimberlite, Pennsylvania, NY – New York Kimberlites, New York, WMMS — White Mountain Magma Series, New Hampshire, MH – Monteregian Hills, Quebec, and the proposed trace of the Great Meteor Hot Spot (GMHS) with associated New England Seamounts. The Appalachian mountains (abbreviated Mtns) are shown in dark grey outline. Line X-X' corresponds to tomography of *Biryol et al.* [2016] in Figure 10.

The youngest magmatic event in the ENAM is the Eocene (47.9 ± 0.2 to 47.0 ± 0.2 Ma) [*Mazza et al.*, 2014] suite of volcanics found in the Valley and Ridge province of northern Virginia-West Virginia (Figure 1) [*Southworth et al.*, 1993]. The Eocene volcanics occur as dikes, sills, plugs, and diatremes up to ~400 m in diameter in at least 150 documented locations [*Southworth et al.*, 1993; *Tso et al.*, 2004; *Tso and Surber*, 2006]. Several hypotheses have attempted to explain the Eocene volcanism: (1) a regional basement fracture zone along the 38th parallel linking volcanism in Kansas to Virginia [*Zartman et al.*, 1967; *Fullagar and Bottino*, 1969; *Dennison and Johnson*, 1971], (2) a still cooling magma chamber which also can account for regional uplift and local warm springs [*Dennison and Johnson*, 1971], (3) a shift in midplate stresses due to plate reorganization [*Vogt*, 1991] (4) a hidden hotspot [*Chu et al.*, 2013], and (5) delamination of an eclogized lower lithosphere or fossilized slab [*Mazza et al.*, 2014]. Lithospheric delamination remains the favored model for the production of the Eocene magmatic event, which can also explain the recent dynamic

topographic uplift experienced in Virginia [*Pazzaglia and Gardner*, 1994; *Miller et al*., 2013; *Rowley et al*., 2013], that left a mantle scar, evident from slow-velocity anomalies under the Virginia-West Virginia Eocene volcanics [*Chu et al*., 2013; *Schmandt and Lin*, 2014; *Biryol et al*., 2016].

3. Materials and Methods

We collected and analyzed 29 new samples from Virginia and West Virginia that expand on previously published data [*Mazza et al*., 2014]. We collected additional mafic and felsic volcanics assumed to belong to the Eocene magmatic pulse, and new mafic and felsic volcanics assumed to belong to the Late Jurassic magmatic pulse. Latitude/longitude locations are reported in supporting information Table S1.

$^{40}Ar/^{39}Ar$ ages were determined at the New Mexico Geochronology Research Laboratory and at the U.S. Geological Survey (USGS) in Reston, Virginia. One biotite separate and two matrix concentrates were prepared for rocks expected to be Eocene in age. These samples were analyzed by the furnace-step heating method at the New Mexico Geochronology Research Laboratory on a Mass Analyzer Products Limited (MAP) 215-50 noble gas mass spectrometer following the standard procedure of this lab [e.g., *McDowell and Harrison*, 1999]. Biotite and amphibole separates were prepared for dikes presumably of Jurassic age. Aliquots of these mineral separates were irradiated in two packages (KD55 & KD57) in the central thimble facility at the TRIGA reactor (GSTR) at the USGS in Denver, Colorado. The monitor mineral used in both packages was FCT-3 sanidine with an age of 27.79 Ma [*Kunk et al*., 1985; *Cebula et al*., 1986] relative to MMhb-1 at 519.4 ± 2.5 Ma [*Alexander et al*., 1978; *Dalrymple et al*., 1981]. Following irradiation the samples were analyzed by the furnace-step heating methods on a MAP 216 mass spectrometer at the USGS in Reston, Virginia. Data reduction was completed following the techniques outlined in *Kunk and McAleer* [2011], *Haugerud and Kunk* [1988], and *Deino* [2001].

Alteration-free rock chips of sample matrices were selected under a stereoscope microscope, powdered in an alumina mill, and fluxed into homogeneous glass disks with ultrapure 34.83% $Li_2B_4O_7$ – 64.67% $LiBO_2$ – 0.5% LiBr flux from Spex® (certified $\ll$1 ppm blank for all trace elements) in the Petrology Lab at Virginia Tech for EDS-XRF and Laser Ablation ICPMS analyses, following the protocols in *Mazza et al*. [2014]. Major element geochemistry was collected on a Panalytical EDS-XRF with a silicon detector at the Department of Geosciences at Virginia Tech. The accuracy for USGS standard BHVO-2 (run as an unknown) was better than 1% for most major elements but Na_2O and P_2O_5 was only better than 8% within reported values. The average relative standard deviation for 10 replicates of BHVO-2 were $<$1% for all major elements except Na_2O and P_2O_5 which were $<$3%. Trace elements from fluxed glasses were collected with an Agilent 7500ce ICPMS coupled with a Geolas laser ablation system following the procedures detailed in *Kelley et al*. [2003] and *Gazel et al*. [2012], with a He flow rate $\sim$1 L/m–5 Hz and an energy density per sample of $\sim$ 7–10 J/cm^2. LA-ICP-MS data were calibrated with fluxed glasses of USGS standards BHVO-2, BCR-2, BIR-1, and STM-1 using Ti from XRF as an internal standard. High precision trace element standard values are from *He et al*. [2015], *Willbold and Jochum* [2005], and *Kelley et al*. [2003] (standard values used reported in supporting information Table S1). The average relative accuracy for 10 replicates of BHVO-2 (run as an unknown) was better than 5% for most trace elements except Sc, Cr, Rb, Y, Zr, Nb, Sn, Ta, Pb, Th, and U (better than 15%). The average precision for BHVO-2 was better 4% for all elements with the exception of Sc, Zn, Sn, and Tm ($<$13%,) (complete statistical analysis reported in supporting information Table S1).

Radiogenic isotope ratios were determined at the Center for Elemental Mass Spectrometry (CEMS), University of South Carolina (USC) following established procedure for this laboratory [*Bizimis et al*., 2013; *Khanna et al*., 2014]. Isotopic ratios for Pb, Nd, and Sr were obtained on a Neptune multi collector ICPMS at USC. Pb isotope ratios were determined by Tl-addition [*White et al*., 2000]. Standard NBS-981 was determined at $^{206}Pb/^{204}Pb = 16.933 \pm 0.001$, $^{207}Pb/^{204}Pb = 15.486 \pm 0.001$, $^{208}Pb/^{204}Pb = 36.682 \pm 0.004$ (2σ, n=10). Isotopic ratios for Nd were normalized to $^{146}Nd/^{144}Nd = 0.7219$ and the Nd standard JNdi was measured at $^{143}Nd/^{144}Nd = 0.512094 \pm 0.000009$ (2σ, n = 8). All Nd measurements are reported relative to JNdi $^{143}Nd/^{144}Nd = 0.512115$. Isotopic ratios for Sr were normalized to $^{86}Sr/^{88}Sr = 0.1194$ and replicate analyses of standard NBS-987 yielded $^{87}Sr/^{86}Sr = 0.710316 \pm 0.000013$ (2σ, n = 7). All Sr measurements are reported relative to NBS-987 $^{87}Sr/^{86}Sr = 0.710250$. USGS standards BCR-2 and BHVO-1 were run as unknowns and are presented in supporting information Table S2. Full procedural blanks ran at Pb $<$ 38pg, Sr $<$ 80pg, and Nd $<$ 10 pg (supporting information Table S2).

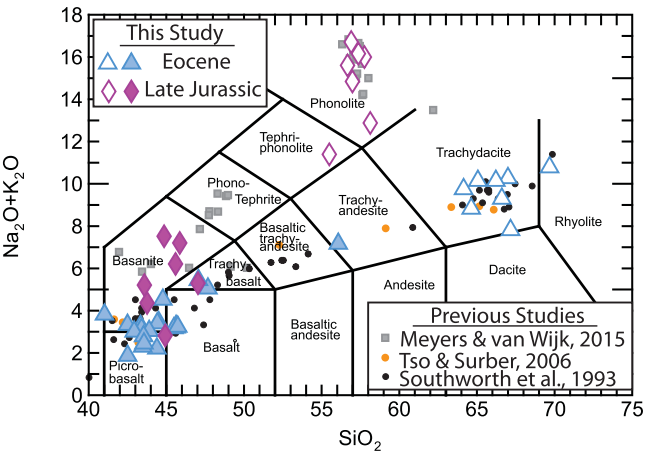

Figure 2. Total alkalis ($Na_2O + K_2O$) versus SiO_2 for the Virginia-West Virginia Late Jurassic and Eocene volcanic pulses showing bimodal populations. Also plotted are Late Jurassic volcanics from *Meyer and van Wijk* [2015] and Eocene volcanics from *Southworth et al.* [1993] and *Tso and Surber* [2006]. Closed symbols representing samples of mafic ($SiO_2 < 50$ wt %) composition and open symbols representing samples of felsic ($SiO_2 > 50$ wt %) composition.

4. Results

4.1. New Geochronological Constraints

$^{40}Ar/^{39}Ar$ ages from Augusta County, Virginia, confirm a Late Jurassic magmatic event ~50 Ma after the rifting of Pangea. High precision $^{40}Ar/^{39}Ar$ biotite and amphibole plateau ages from sample 39 (Figure 1) are 152.7 ± 0.4 Ma and 153.3 ± 0.4 Ma, respectively (supporting information Figures S1a and S1b). These mineral separates yield integrated ages of 152.5 ± 0.5 Ma, and 152.2 ± 0.4 Ma, respectively. Biotite and amphibole were also dated from sample 35 and yielded slightly disturbed age spectra (supporting information Figures S2a and S2b). However, these samples yield preferred ages of 153.4 ± 1.0 Ma and 152.9 ± 0.7 Ma, and suggest alkali magmatism occurred over a short period of time (<1 Ma) at 152–153 Ma.

$^{40}Ar/^{39}Ar$ analyses for the Eocene magmatic event include biotite dated from sample 22b which yields an age of 48.79 ± 0.07 Ma (supporting information Figure S3) and is the location as 22a, which yields an age of 47.0 ± 0.2 Ma (amphibole) [*Mazza et al.*, 2014]. Matrix from sample 6 (basalt) yields an age of 48.6 ± 1.0 Ma (supporting information Figure S4). Matrix from sample 2 (basalt) was also dated and yields slightly disturbed age spectra (supporting information Figure S5) but the preferred ages of 48.78 ± 0.89 Ma and 47.39 ± 0.60 Ma are consistent with the other reported ages for the Eocene event [*Mazza et al.*, 2014].

4.2. Geochemistry of the Late Jurassic Magmatism

There are two populations of samples, relatively low silica (SiO_2 44–47 wt %) and high silica (SiO_2 56–58 wt %). The low silica samples (Figure 2) have varying textures from porphyritic to aphanitic. Porphyritic samples are characterized by fine-grained matrix with phenocrysts of pyroxene + nepheline ± olivine ± amphibole ± biotite ± apatite. Amphibole and pyroxene phenocrysts are zoned with smooth, rounded edges, but show no other signs of reabsorption (supporting information Figures S6a and S6b). Some pyroxenes have altered cores, and can be as large as 4 mm. Crustal xenoliths are common in the low silica samples. Like the Late Jurassic mafic suite, the high silica samples range from aphanitic with no phenocrysts to having abundant amphibole (0.7–2.5 mm) + biotite (<0.6 mm) + nepheline ± K-feldspar phenocrysts (<7 mm) (supporting information Figure S6c). Amphibole phenocrysts in the high silica samples are defined by sharp crystal edges and range from (supporting information Figure S6d). In some cases, K-feldspar phenocrysts exhibit tartan plaid twinning. Nepheline and feldspars in the groundmass generally form blades that are elongate to paleoflow direction. For more detailed petrographic descriptions for these samples, see *Johnson et al.* [1971].

Primitive mantle normalized spider diagrams show enrichments in Ba, but some show depletions in other fluid-mobile elements (Rb, K, and U) and a negative slope in the heavy rare earth elements (HREE) (Figure 3a). The Jurassic mafic samples are more enriched in high field strength elements (e.g., Nb 128–164 ppm, Ta 6–7ppm, Zr 168–297ppm) than average ocean island basalt (OIB) and plot in the upper end of the OIB field in the mantle array (Figure 4a) [*Pearce*, 2008]. Ce/Pb values straddle the canonical OIB values (~25), while Nb/U show greater variability, ranging from average OIB-concentrations to more enriched values (Figure 4b) [*Hofmann et al.*, 1986]. These volcanics are also characterized by enrichments in Gd/Yb and La/Yb (Figure 4c).

The Late Jurassic felsic samples are predominantly classified as phonolites, with one tephriphonolite (Figure 2). These phonolites are extremely enriched in high field strength elements (e.g., Nb 239–710 ppm,

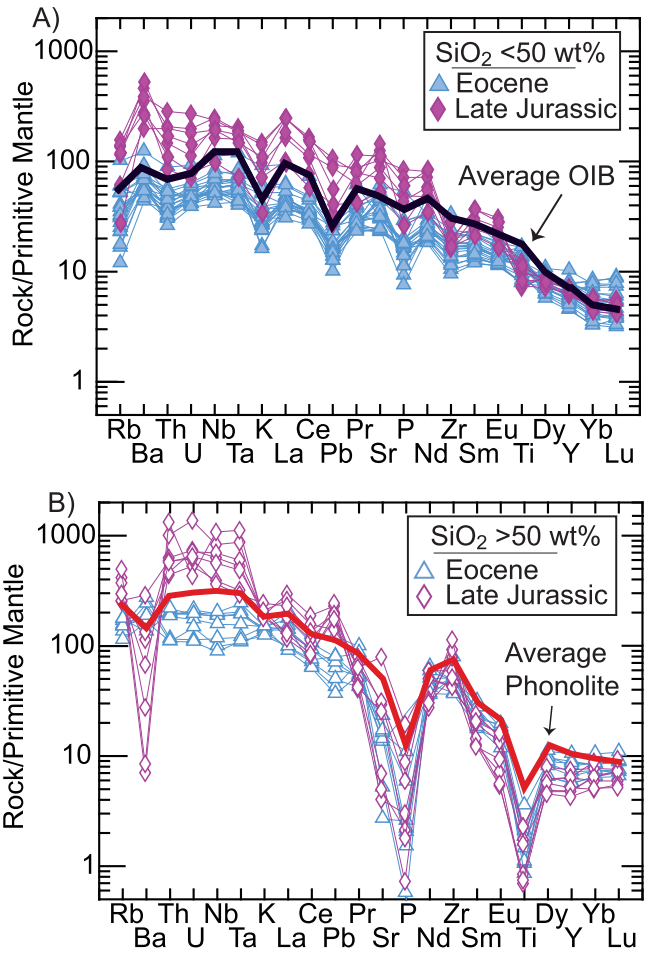

Figure 3. Primitive mantle [from *McDonough and Sun*, 1995] normalized spider diagrams for (a) Eocene and Late Jurassic volcanics of mafic composition ($SiO_2 < 50$ wt %) with average OIB calculated from the GEOROC database, and (b) Eocene and Late Jurassic volcanics of felsic composition ($SiO_2 > 50$ wt %) with average global nonsubduction-influenced phonolites calculated from the GEOROC database.

Ta 11–41 ppm, Zr 444–1190 ppm) compared to the average nonsubduction influenced phonolites. The general primitive normalized pattern for the Virginia-West Virginia phonolites shows depletions in Ba, Sr, P, and Ti, an enrichment in Pb, and a flat/slight positive slope in HREE (Figure 3b).

Sr-Nd-Pb isotopic analyses from one trachybasalt and four phonolites are plotted in Figure 5 (supporting information Table S2). The range of radiogenic isotopic ratios for the Late Jurassic event, age corrected to 150 Ma, are $(^{87}Sr/^{86}Sr)_i$ 0.704170–0.711616, $(^{143}Nd/^{144}Nd)_i$ 0.512459–0.512546, $(^{206}Pb/^{204}Pb)_i$ 18.630–22.646, $(^{207}Pb/^{204}Pb)_i$ 15.562–15.792, and $(^{208}Pb/^{204}Pb)_i$ 38.21640.141.

It is important to note that sample 32, previously used in *Mazza et al*. [2014], has been regrouped from the Eocene suite to the Jurassic suite, based on geographic location, trace element enrichments, and $^{144}Nd/^{143}Nd$ radiogenic isotopes.

4.3. Geochemistry of the Eocene Magmatism

The Eocene mafic samples range from picrobasalt to basalt (41–48 wt % SiO_2, Figure 2, supporting information Table S1). The mafic samples are generally porphyritic with fresh olivine (0.2–1 mm) + clinopyroxene (<7 mm) + spinel (< 0.1 mm) phenocrysts (supporting information Figure S7a). Some samples also contain mantle clinopyroxene and olivine xenocrysts and plagioclase microphenocrysts [*Sacco et al*., 2011]. The mafic units are generally better preserved in the field, found as dikes, sills, and volcanic plugs. The felsic samples are aphanitic to porphyritic with fresh biotite (<2 mm) ± amphibole (<0.5 mm) and somewhat altered plagioclase and alkali feldspar phenocrysts (supporting information Figures S7b and S7c). Amphibole and biotite generally have well-defined crystal edges.

Trace elements normalized to primitive mantle show a typical intraplate signature (Figure 3c) that includes a steep slope in the HREE, with enrichments in Gd/Yb and La/Yb (supporting information Table S1, Figures 3c and 4c). Positive enrichments are found in high field strength elements (e.g., Nb 27–107 ppm, Ta 1–6 ppm, Zr 98–252 ppm) and depletions are found in fluid mobile elements (e.g., K and Pb). These mafic volcanics also fall within the OIB region of the mantle array (Figure 4a) [*Pearce*, 2008] and are close to canonical OIB Ce/Pb and Nb/U values (Figure 4b) [*Hofmann et al*., 1986].

The felsic samples range in composition from trachyandesite to rhyolite (SiO_2 56–69 wt %, Figure 2). Like the mafic samples, high field strength elements are enriched (Figure 3d), but the HREE show a flat slope as also noted in samples from the Jurassic event. Dy/Yb ratios are also lower than the mafic volcanics, which is attributed to amphibole differentiation [*Davidson et al*., 2007].

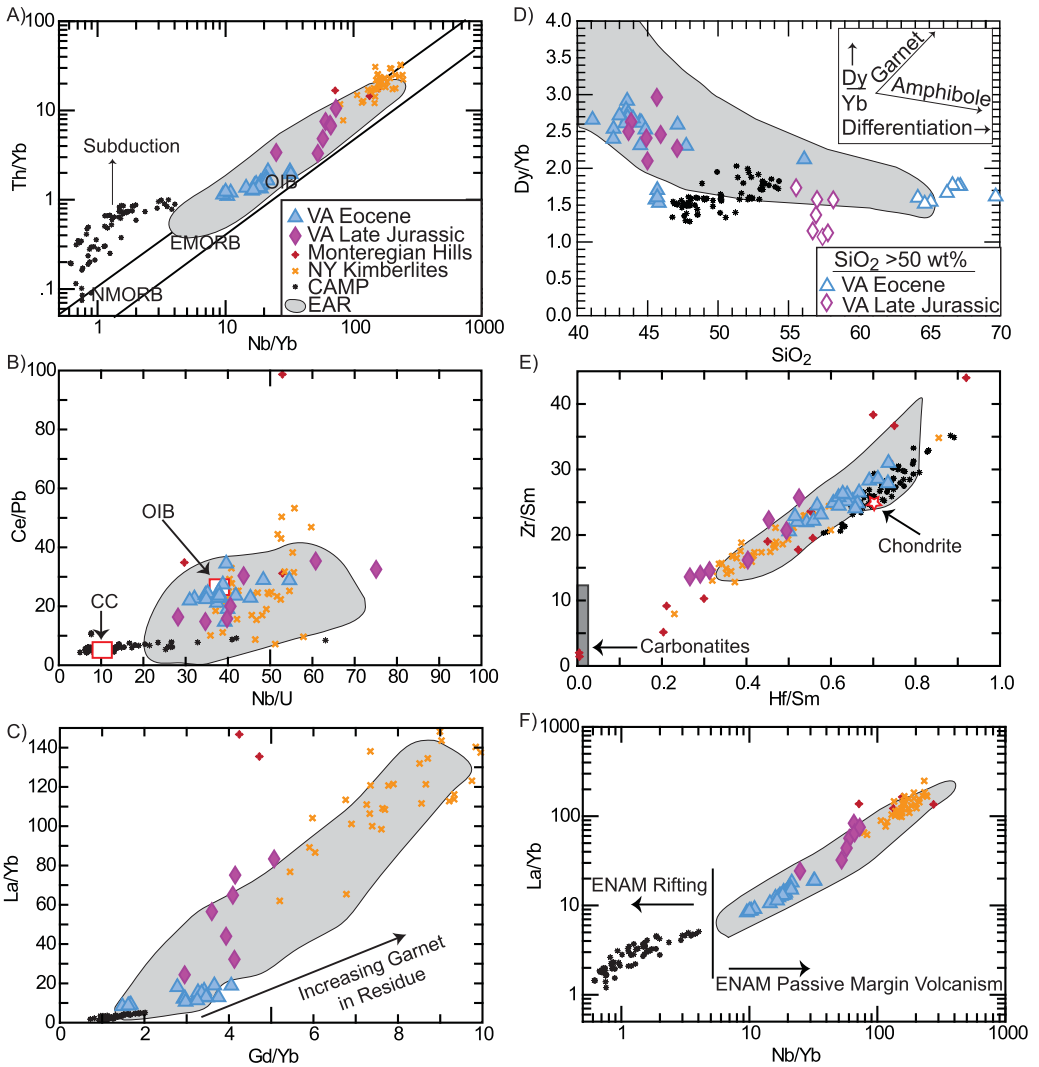

Figure 4. (a) Mantle array diagram from *Pearce* [2008] showing the regions for NMORB (Normal Mid Ocean Ridge Basalt), EMORB (Enriched Mid Ocean Ridge Basalt), OIB (Ocean Island Basalt), and subduction influence. (b) Ce/Pb versus Nb/U to show conical continental crust (CC) and OIB concentrations [*Hofmann et al*., 1986]. (c) La/Yb versus Gd/Yb to show correlation of increasing Gd/Yb and increasing garnet in residue. (d) Dy/Yb versus SiO_2 to show amphibole fractionation [*Davidson et al*., 2007] (e) Zr/Sm versus Hf/Sm modified from *Dupuy et al*. [1992] to show trends to carbonatite metasomatism. (f) La/Yb versus Nb/Yb shows differences in ENAM rifting and passive margin volcanics. The East African Rift volcanics (EAR) are shown in a field, whereas southeast Brazil, Central Atlantic Magmatic Province (CAMP), NY Kimberlities, and Monteregian Hills are shown individually.

5. Discussion

5.1. Petrological Modeling to Evaluate Magma Evolution

The composition of the most primitive mafic volcanics is useful for understanding where the magmas equilibrated in the mantle, but to better understand mafic to felsic magma evolution we conducted geochemical modeling using rhyoliteMELTS [*Gualda et al*., 2012]. Calculations were completed for crystal fractionation beginning from the liquidus and then cooling at 5°C temperature intervals at constant pressure.

Ideally, the most primitive mafic composition should be the starting composition for fractional crystallization. However, the most primitive composition for the Late Jurassic volcanics failed to produce fractional crystallization models that reproduced the data, and thus we conducted our models with a range of starting compositions. The average composition of the mafic Late Jurassic volcanics produced melting models that best correspond to the compositions of the phonolites. For the Late Jurassic event, a variety of starting pressures, water contents, and oxygen fugacities (fO_2, buffered with fayalite-magnetite-quartz, FMQ) were used in the models, with 10 kbar/35 km and 1 wt % H_2O producing the fractional crystallization paths that

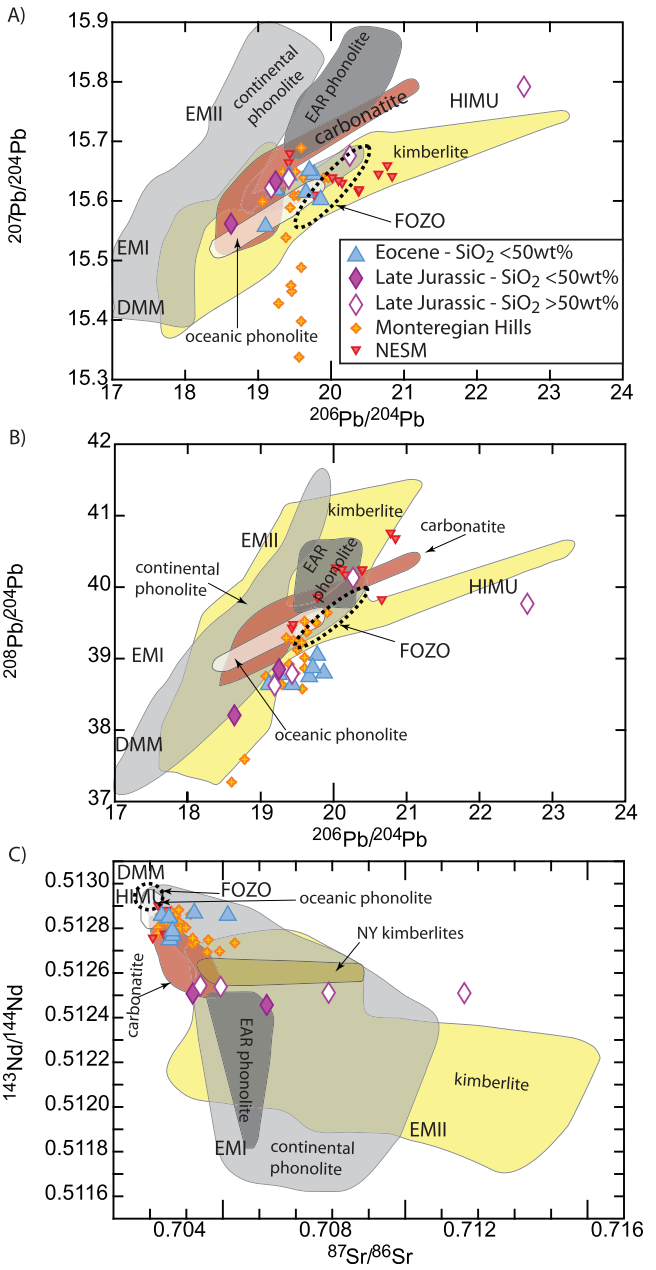

Figure 5. Radiogenic isotope results for ENAM volcanics with the first reported Pb-Sr-Nd systematics for the Virginia Late Jurassic volcanics. ENAM volcanics are compared with East African Rift (EAR) phonolites, continental phonolites, oceanic phonolites, carbonatites, and kimberlites (data obtain from the GEOROC database; georoc.mpch-mainz.gqdq.de/georoc/). Virginia samples were age corrected to 150 Ma (late Jurassic) and 50 Ma (Eocene). DMM – depleted MORB mantle, EMI – enriched mantle I, EMII – enriched mantle II, HIMU – high μ, FOZO – Focus Zone [*Zindler and Hart*, 1986; *Stracke et al*., 2005].

correspond with our data (Figure 6). While the water contents remain unknown for the Late Jurassic event, 1 wt % water is a reasonable estimate given the presence of hydrous phases such as amphibole and biotite, and the ability of phonolitic melts to contain 0.7–4.9 wt % water [*Carroll and Blank*, 1997; *Di Muro et al*., 2006]. Using an fO_2 FMQ buffer, we produce models for fractional crystallization that best reproduce the evolution from basanite to phonolite (Figure 6a). As the biotite and K-feldspar were successfully crystallized in our models, but it failed to crystallize amphibole, which is a common limitation of rhyoliteMELTS [*Gualda et al*., 2012]. Besides failing to crystalize amphibole, nepheline did not crystallize in these models which potentially is viable with the increase in Al_2O_3 that the phonolites exhibit but the models do not reproduce (Figure 6b). The other possibility to explain this difference in Al_2O_3 between the models and observed compositions is magmatic recharge. However, we do not see textural indicators of reabsorption in the samples.

For the Eocene event, we modeled a variety of starting compositions, pressures, water contents, and fO_2 values. The most primitive Eocene mafic sample (10) yielded models at 2 kbar/7 km and 1 wt % H_2O that best reproduced the data trends. Models with 1 wt % H_2O are within the range of magmatic H_2O calculated for the Eocene magmas [*Sacco et al*., 2011; *Soles et al*., 2014]. FMQ best reproduced the majority of the fractionation trends of the felsic samples (Figure 6), especially MgO and FeO* (Figure 6d). However, in order to reproduce the alkali content of the trachydacites/rhyolites, the buffer FMQ +3 was necessary. This could be a limitation of the model because of its inability to produce thermodynamically complex phases, such as amphibole. Amphibole fractionation could explain the flat trend in Al_2O_3 versus MgO space that the rhyoliteMELTS fails to reprodue (Figure 6b).

5.2. Assessment of Crustal Interaction

Crustal contamination has the potential to affect the trace element and isotopic compositions of the Late Jurassic and Eocene volcanics. *Mazza et al*. [2014] showed that the Eocene mafic volcanics were not affected by crustal contamination by conducting assimilation-fractional crystallization (AFC) model calculations

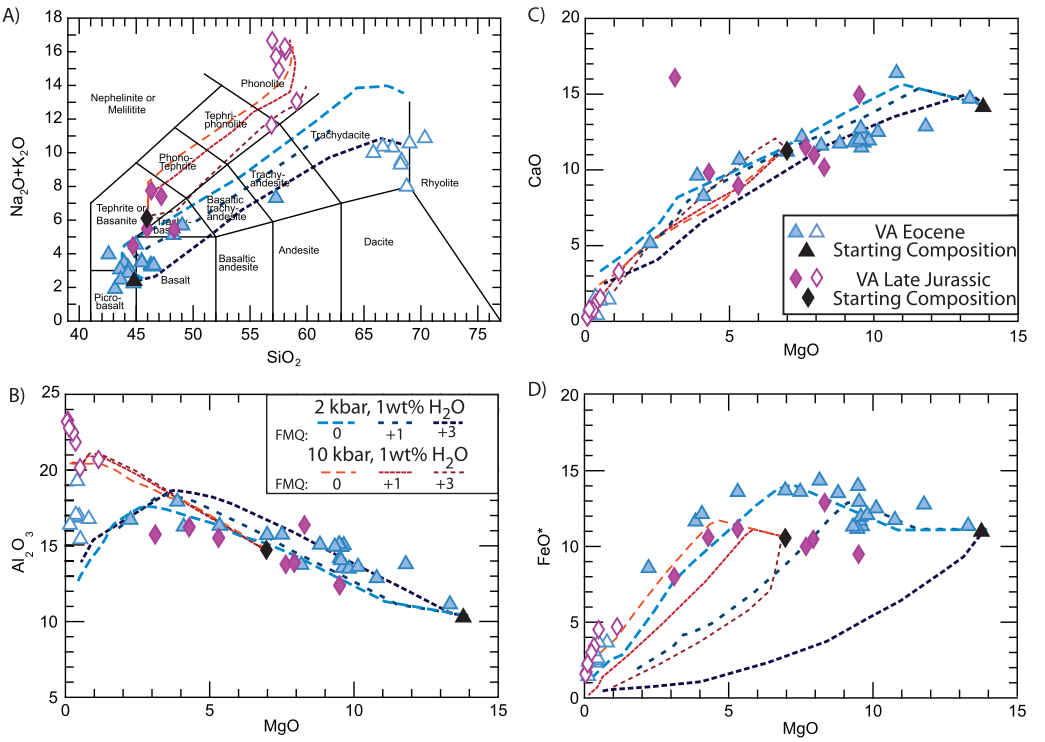

Figure 6. Fractional crystallization models made with rhyoliteMELTS [*Gualda et al.*, 2012], showing various fractional crystallization paths of the melt for both the Virginia Eocene and Late Jurassic magmas. The starting compositions are indicated by black diamond/triangle, with varying oxygen fugacity buffer conditions (fO_2 FMQ) indicated by variation of line texture.

[*DePaolo*, 1981]. To assess if any crustal material was assimilated during the evolution of the Late Jurassic event, we conduct similar AFC modeling. For the mafic end-member, we used the most primitive sample with isotopic data, 32, which has a modal composition of 10% olivine, 30% clinopyroxene, and 60% plagioclase. We used the most primitive sample because we are interested in how these magmas evolve to more felsic compositions, and if the more felsic compositions share isotopic signatures with the regional basement. Using the modal compositions and parameters for bulk trace-element partition coefficients for Sr, Nd, and Pb [*Rollinson*, 1993; *McKenzie and O'Nions*, 1991], we calculated partition coefficients of 1.12 for Sr, 0.10 for Nd, and 0.22 for Pb. Trace element compositions for the Late Jurassic volcanics and the basement material used in the AFC models are similar (supporting information Table S3). A limited data set of isotopic compositions for local Blue Ridge crustal basement consisting of gneisses, diorite-granites, and charnokites was used for the assimilant composition [*Pettingill et al.*, 1984; *Sinha et al.*, 1996]. We modeled AFC for the extreme isotopic end-members (RM1, lowest $^{87}Sr/^{86}Sr$; S-3-81, highest $^{87}Sr/^{86}Sr$; JP-92-36, most enriched Pb) and for the average composition of local Blue Ridge basement, from the Pedlar and Lovingston Massifs approximately 50 km to the southeast of the Late Jurassic volcanics, and the average regional Blue Ridge basement from Georgia, South Carolina, North Carolina, and Virginia [*Sinha et al.*, 1996; *Samson et al.*, 1995; *Carrigan et al.*, 2003].

The regional and local Blue Ridge basement is dominated by unradiogenic lead ($^{206}Pb/^{204}Pb < 17.6$ and $^{208}Pb/^{204}Pb < 37.5$) such that AFC fails to explain the trend for the Late Jurassic enriched composition ($^{206}Pb/^{204}Pb < 22.646$ and $^{208}Pb/^{204}Pb < 40.141$) (Figures 7a and 7b). Even when considering the isotopic end-members, AFC fails to explain the enriched Pb compositions of the Late Jurassic volcanics (Figures 7a and 7b). Nd for the Late Jurassic volcanics is fairly consistent (average $^{143}Nd/^{144}Nd = 0.51250$) and generally more radiogenic than the local basement (average $^{143}Nd/^{144}Nd = 0.51221$). While a few basement samples are within the range of the Late Jurassic volcanics, AFC using the average basement composition cannot account for the radiogenic $^{143}Nd/^{144}Nd$ measured in the Late Jurassic volcanics (Figure 7c). The Late Jurassic volcanics share a similar range of $^{86}Sr/^{87}Sr$ as the Virginia basement material, and AFC modeling suggests up to 30% assimilation of basement material can influence the Sr compositions of these volcanics. However,

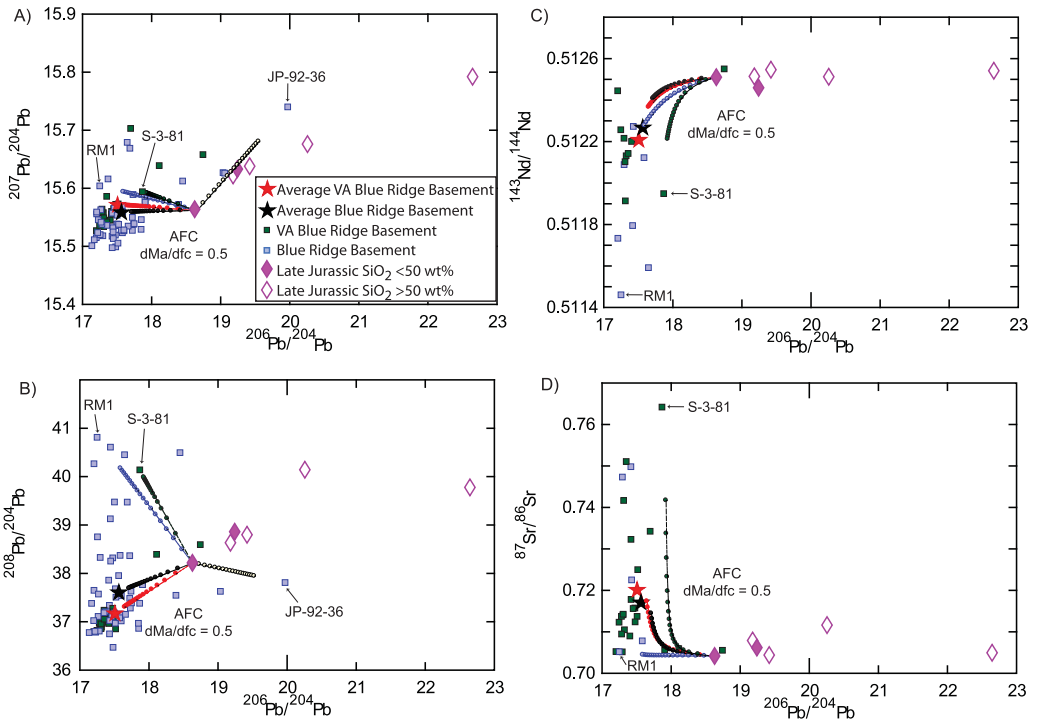

Figure 7. Assessment of crustal interaction. Blue Ridge basement from *Pettingill et al.* [1984], *Samson et al.* [1995], *Sinha et al.* [1996], and *Carrigan et al.* [2003]. Basement end-members are RM1 [*Carrigan et al.*, 2003], S-3-81 [*Pettingill et al.*, 1984], and JP-92-36 (Pb only) [*Sinha et al.*, 1996]. All samples are age corrected to average eruptive age of Virginia Late Jurassic magmatism (150 Ma). Every circle-tick mark represents dF = 0.05 with a maximum dF = 1. F = mass of assimilated material over initial mass. The rate of assimilation to crystallization (R = dMa/dfc) is 0.5.

when comparing Sr with the other isotopic systems, AFC cannot account for the trends of $^{87}Sr/^{86}Sr$ versus $^{206}Pb/^{204}Pb$ (e.g., Figure 7d), $^{87}Sr/^{86}Sr$ versus $^{207}Pb/^{204}Pb$, $^{87}Sr/^{86}Sr$ versus $^{208}Pb/^{204}Pb$, or $^{87}Sr/^{86}Sr$ versus $^{143}Nd/^{144}Nd$.

The evolution from the most primitive mafic sample with isotopic data to the most evolved phonolite does not seem to be controlled by interaction with the basement material, and in fact plots in the opposite direction from crustal interaction. However, we must be careful with these interpretations for three reasons, (a) the availability of complete Sr-Nd-Pb radiogenic isotopes and trace element abundances for regional crustal basement is limited, and (b) it is not certain that the lower crust beneath the Appalachians is the same as the basement massifs [*Pettingill et al.*, 1984; *Sinha et al.*, 1996], (c) we cannot rule out AFC with carbonate crust, as this area of Virginia-West Virginia has abundant carbonates, but we cannot model AFC with these regional carbonates due to the lack of complete trace element and radiogenic isotopic data [e.g., *Samson*, 1996 which lacks trace element concentrations].

5.3. Contrasting the Record of Late Jurassic and Eocene Events in Virginia-West Virginia

The Late Jurassic and Eocene magmatic events both range from mafic (basanite or picrobasalt) to felsic (phonolite or rhyolite) compositions (Figure 2). The mafic rocks from both events share intraplate signatures with enrichments in LILE and Nb/Yb and Th/Yb ratios. Heavy REE are good indicators of garnet in the residue, as seen by both the steep slope of HREE (Figures 3a and 3c) and high Gd/Yb ratios (Figure 4c). Therefore, both the Virginia-West Virginia Late Jurassic and Eocene mafic volcanics have HREE signatures indicative of melt originating at depths with residual garnet (>2.5–3 GPa, e.g., *Johnson* [1998] and *Salters et al.* [2002] for peridotite mantle and 1.8–5 GPa for pyroxenite mantle, e.g., *Liu and Presnall* [2000]; *Tuff et al.* [2005]). The Late Jurassic mafic pulse has higher concentration of LREE than the Eocene pulse (La/Yb > 83 versus 19, respectively), as well as high field strength elements (Nb/Yb > 73 versus 32, respectively) suggesting that they resulted from lower degrees of partial melting or a more enriched source in incompatible elements. Ce/Pb and Nb/U values are close to the canonical OIB value (Figure 4b) [*Hofmann et al.*, 1986], suggesting an asthenospheric source with limited interaction with the continental crust for

both events. The enrichments of Nb/U are greater for the Late Jurassic event, which could suggest small melt fractions. Similarly, the Late Jurassic phonolites are also more enriched in LILE than the Eocene felsic rocks, and are characterized by depletions in Ba, Sr, P, and Ti. Depletions in Ba, Sr, and Eu are indicative of feldspar fractionation (Figure 3b) while lower P and Ti concentrations probably resulted from fractionation of apatite and Ti-oxides, respectively. The felsic volcanics from the Eocene event do not share the Ba and Eu depletions (Figure 3d). The rhyoliteMELTS models for the Late Jurassic volcanics produced K-feldspar during late stage fractionation, which agrees with the presence of K-feldspar phenocrysts and the trace element chemistry.

Radiogenic isotopic data show clear differences in the two pulses of magmatism in Virginia-West Virginia. We age-corrected Sr-Nd-Pb isotopes of the Late Jurassic volcanics to 150 Ma (supporting information Table S2, Figure 5). Additionally, the ENAM isotopic values are shown with global data for phonolites from continental intraplate, rift (East African Rift; EAR) and oceanic settings, kimberlites (Circum-Parana, Serbia, Canada, Baltic Shield, and New York), carbonatites, New England Seamounts, and Monteregian Hills, in order to elucidate processes that could have been responsible for volcanism. Radiogenic isotopes are indicators of melts derived from various mantle reservoirs, which have been defined as depleted mid-ocean ridge basalt mantle (DMM), enriched mantle I and II (EMI and EMII), and high μ ($\mu = {}^{238}U/{}^{204}Pb$) mantle (HIMU) [*Zindler and Hart*, 1986]. The Late Jurassic alkaline volcanics cover a larger range of $({}^{206}Pb/{}^{204}Pb)_i$ versus $({}^{207}Pb/{}^{204}Pb)_i$ space than the Eocene pulse, with the phonolites extending toward radiogenic Pb-isotopes with HIMU affinities. The extent of radiogenic $({}^{206}Pb/{}^{204}Pb)_i$ ratios is well beyond the typical range of silicate magmas. The only other locations with similar enrichments in ${}^{206}Pb/{}^{204}Pb$ are kimberlites from Circum-Parana and carbonatites from the EAR. The high ${}^{206}Pb/{}^{204}Pb$ values from Circum-Parana have not been adequately explained, but the overall isotopic signatures suggest lithospheric mantle interaction common to kimberlites [*Araujo et al*., 2001]. Enrichments in ${}^{208}Pb/{}^{204}Pb$ can be interpreted as interaction with an enriched mantle (EMII) component (Figure 5b). Kimberlites from the Baltic Shield and Serbia, and carbonatites and phonolites from the EAR have similar enrichments in ${}^{206}Pb/{}^{204}Pb$ and ${}^{208}Pb/{}^{204}Pb$ ratios. Overall, the variable enrichments in ${}^{208}Pb/{}^{204}Pb$ relative to ${}^{206}Pb/{}^{204}Pb$ suggest that the ENAM Late Jurassic alkaline volcanics contained EMII and HIMU components in their source, while the Eocene event suggests mixing between a HIMU and DMM component [*Mazza et al*., 2014].

Late Jurassic alkaline volcanics in the ENAM have relatively uniform $({}^{143}Nd/{}^{144}Nd)_i$ values, while $({}^{87}Sr/{}^{86}Sr)_i$ covers a wide range from relatively unradiogenic to radiogenic (Figure 5c). These compositions are very similar to the New York kimberlites, which have been interpreted as derived from the asthenospheric mantle [*Bailey and Lupulescu*, 2015]. The enrichments in ${}^{87}Sr/{}^{86}Sr$ are potentially related to crustal interaction or calcite alteration.

As previously discussed, AFC cannot adequately explain the trends of Sr-Nd-Pb systematics for the Late Jurassic volcanics. Instead Sr-Nd-Pb systematics show an enrichment of radiogenic Pb with magma evolution, and ${}^{87}Sr/{}^{86}Sr$-${}^{143}Nd/{}^{144}Nd$ compositions on par with volatile-rich lithologies, e.g., kimberlites and carbonatites. We interpret these trends as the melting of an EMII influenced mantle source similar to the source of the New York kimberlites to the north, the interaction with an unsampled high ${}^{206}Pb/{}^{204}Pb$ source potentially associated with metasomatism typical to kimberlite/carbonatite magmas.

5.4. Origin of Cogenetic Felsic Rocks Associated With the Postrift Mafic Pulses

A previous study interpreted these Late Jurassic volcanics as low and high silica adakites [*Meyer and van Wijk*, 2015]. Adakites were defined by *Defant and Drummond* [1990] as subduction-related intermediate to felsic rocks, though further evidence also suggests that not all adakites are subduction related since partial melting of delaminated continental crust can also produce adakite compositions [*Xu et al*., 2002]. Adakites usually crystallize plagioclase, hornblende, and biotite, and have low Y and Yb (<18 and 1.9 ppm, respectively), high Mg# (molar[MgO/(MgO + FeO)]*100)) of ~51, high $(La/Yb)_N > 10$ [*Martin*, 1999], and high Sr/Y [*Defant and Drummond*, 1990].

Some trace element signatures of Virginia-West Virginia Late Jurassic volcanics resemble adakites, as both the high silica and low silica rocks have high $(La/Yb)_N$ (Figure 8a) and high Sr/Y (Figure 8b), well within the range of global adakites. However, Yb_N and Y values are higher than the global adakite composition. In addition, the Mg# (Figure 8c) of the high silica volcanics is <20, thus significantly lower than the expected Mg# of adakites.

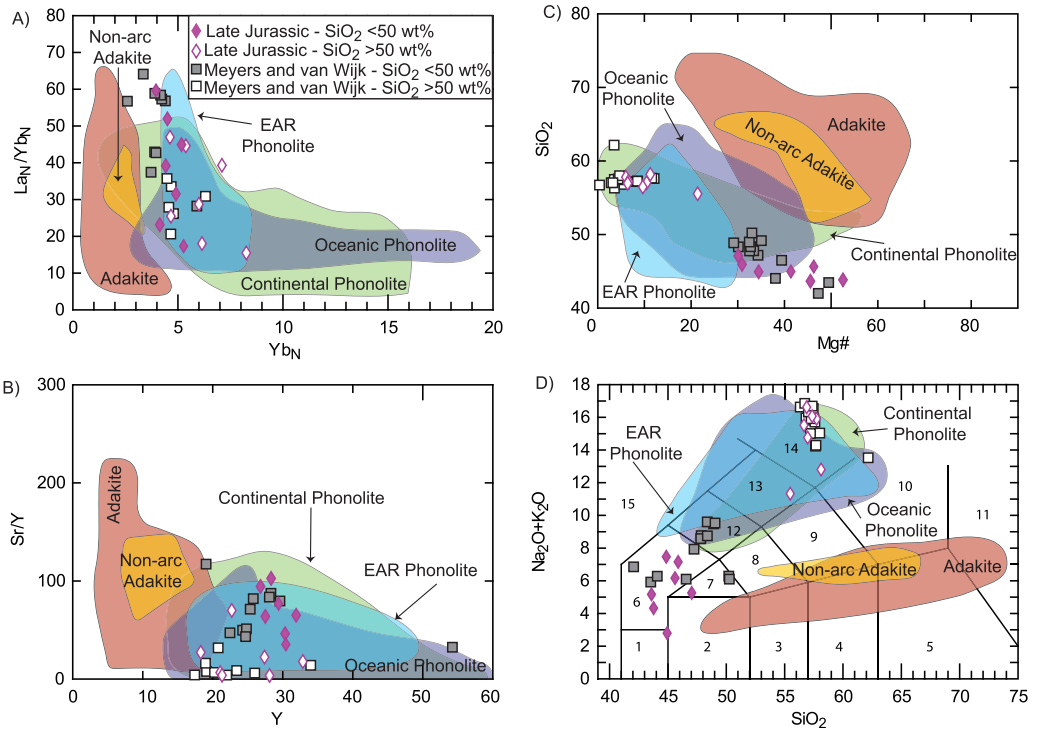

Figure 8. Adakite discriminatory plots with global adakites, nonarc adakites, continental phonolites, East African Rift (EAR) phonolites, and oceanic phonolites from GEOROC database. (a) Chondrite normalized La/Yb versus Yb [*Martin*, 1999]. (b) Sr/Y versus Y [*Defant and Drummond*, 1990]. (c) SiO_2 versus Mg# where Mg# = molar MgO/(MgO + FeO)*100. D) Total alkalis ($Na_2O + K_2O$) versus SiO_2 verse with rock types as 1: Picrobasalt, 2: Basalt, 3: Basaltic Andesite, 4: Andesite, 5: Dacite, 6: Basanite, 7: Trachybasalt, 8: Basaltic Trachyandesite, 9: Trachyandesite, 10: Trachydacite, 11: Rhyolite, 12: Phonotephrite, 13: Tephriphonolite, 14: Phonolite, and 15: Melilitite.

We instead interpret these rocks as phonolites, which are more enriched in Yb_N versus $(La/Yb)_N$ (Figure 8a) and Y versus Sr/Y (Figure 8b) than adakites. We restricted the geochemical data downloaded from GEOROC to high precision geochemistry that included the full range of trace elements (in particular Nb and Ta), and then subdivided the data to continental, rift (EAR), and oceanic phonolites. All three types of phonolites have high $(La/Yb)_N$ and high Sr/Y, similar to what is expected for adakites. However, Yb_N and Y are significantly more enriched in phonolites than in adakites. In general, the and high silica Late Jurassic volcanics predominantly correspond to phonolites from the EAR and ocean islands. The Mg# of these rift and intraplate phonolites is also within the range of the high silica Late Jurassic volcanics. Nb and Ta are potentially the most important elemental pair to help distinguish subduction versus nonsubduction magmas, due to the depletions of Nb and Ta in subduction related magmas. Arc-related adakites have strong depletions in Nb and Ta relative to other elements of similar compatibility [*Maury et al.*, 1996]. *Meyer and van Wijk* [2015] did not report any Nb or Ta data in their study, and thus could not use these elements to further help constrain their interpretation. As mentioned above, we found that Late Jurassic volcanics are highly enriched in Nb and Ta (Figures 3a and 3b), which is strong evidence for our reinterpretation of these rocks as nonsubduction-influenced phonolites. The alkali contents and mineral chemistry can also help determine adakites verses phonolite compositions, with the major element compositions of adakites being more similar to andesite-dacites whereas phonolites are enriched in alkalis (Figure 8d) [*Streckeisen*, 1979] and the preferred fractionation of feldspars in adakites and feldspathoids in phonolites. The Late Jurassic volcanics are enriched in Na_2O and K_2O and fractionated nepheline, both common features of phonolites.

Highly evolved alkaline lavas such as phonolites can be produced by several processes: fractional crystallization [e.g., *Panter et al.*, 1997], assimilation fractional crystallization (AFC) [e.g., *Wiesmaier et al.*, 2012], and variable degrees of partial melting [e.g., *Pelleter et al.*, 2014]. Fractional crystallization is most frequently evoked for producing phonolites in both rift and intraplate environments [e.g., *Panter et al.*, 1997; *Weaver*, 1990; *Le Roex et al.*, 1990; *Holm et al.*, 2005]. The EAR has phonolitic and carbonatitic magmas found within proximal to each other, including Oldoinyo Lengai, the only active carbonatitic volcano [*Bell and Simonetti*, 1996].

Phonolites in the EAR are characterized by depletions in Ba, P, Ti, and enrichments in Nb, Y, Hf, Th, and Ta [*Klaudius and Keller*, 2006; *Mana et al*., 2012] and are suggested to have formed by crystal fractionation from nephelinite. Phonolites from Marie Byrd Land, the continental rift in Antarctica, have also been explained by fractional crystallization of a basanitic magma source [*Panter et al*., 1997; *LeMasurier et al*., 2011].

Crystal fractionation has also been the proposed mechanism for the evolution of basanitic to phonolitic magmas in intraplate settings, such as seen in Trindade [*Weaver*, 1990; *Siebel et al*., 2000], Tristan da Cunha [*Le Roex et al*., 1990], Kerguelen [*Weis et al*., 1993], and Cape Verde [*Holm et al*., 2005]. Like rift phonolites, these evolved lavas have enrichments in Nb, Ta, Zr, and Hf and depletions in Ti. However, Tenerife in the Canary Islands and Mayotte in the Comoros Islands are two intraplate settings with evolved phonolites that cannot be adequately explained by fractional crystallization, where AFC and/or recycling of crustal material has been proposed [*Wiesmaier et al*., 2012].

Based on our petrological modeling using rhyoliteMELTS (Figure 6), fractional crystallization from a basanitic magma source could have produced the Late Jurassic phonolites. The evolved nature of these phonolites makes constraining melting conditions difficult with traditional geothermobarometers. Nevertheless, one mafic sample can be used to estimate temperatures of melt equilibration with the *Lee et al*. [2009] thermobarometer, as it is based on olivine-melt Fe-Mg exchange for temperature calculations, and Si activity in melt in equilibrium with orthopyroxene + olivine for pressure calculations. Sample 31 was the only sample to crystallize olivine (sample 31) yielding melt equilibration conditions of 1351°C and 2.09 GPa/70 km. Fractional crystallization models suggest that the phonolites equilibrated around 1 GPa, or approximately 35 km depth. This places the final stages of fractional crystallization at the base of the crustal lithosphere, assuming an average crustal thickness of 40 km. Trace element signatures for the Late Jurassic phonolites agree with a shallow region of crystallization due to the flat/slight positive slope in HREE (Figure 3b) and a low Dy/Yb ratio (Figure 4d), consistent with the presence of amphibole in cumulate phases [e.g., *Davidson et al*., 2007].

Our models (Figure 6) show that the Eocene trachydacites and rhyolites are likely the result of crystal fractionation at shallow pressures. Modeling crystallization conditions suggest that these magmas differentiated at 0.2 GPa/6 km. HREE signatures confirms a shallow crystallization depth, seen by a flat slope in HREE (Figure 3d) that potentially obscured the original source-related signatures. Amphibole fractionation with an overall higher SiO_2 concentration also confirms crystallization at shallow depths (Figure 4d). This modeling exercise shows that the Eocene and Late Jurassic events fractionated at different depths, likely due to the difference in source compositions. The common association of phonolites with carbonatites, and the similarities of the Late Jurassic radiogenic isotopic data with volatile-rich lithologies, e.g., carbonatites and kimberlites, suggests that carbonatite metasomatism could be responsible for composition of the Late Jurassic volcanics.

5.5. Wide-Spread Alkaline Magmatic Pulses in the Late Jurassic Along the ENAM

New England and the adjacent Montréal region of Canada have also experienced multiple pulses of magmatic activity since the breakup of Pangea recorded by the White Mountain Magma Series (WMMS) from 200 to 90 Ma [*Foland and Faul*, 1977; *Hubacher and Foland*, 1991], the Monteregian Hills volcanic province in Montréal at 124 Ma [*Foland et al*., 1986], and the New England Seamounts (NESM) with a clear west-east age progression from 103 to 82 Ma [*Duncan*, 1984] (Figure 9). The multiple pulses of magmatism in New England have been linked to the movement of the Great Meteor hotspot [e.g., *Eby*, 1985], however, all events except the NESM lack a clear age progression which argues against a common source.

Even if the WMMS, Monteregian Hills, and the NESM are not all the products of the Great Meteor hotspot, these volcanics and the Virginia-West Virginia volcanics can help elucidate processes involved with postrift magmatism of the ENAM. Limited data exists for the postrift New England volcanics, but what is available suggests an alkaline affinity. The Monteregian Hills range from alkali basalts to carbonatites (Oka carbonatite complex in the west) [*Eby*, 1985; *Roulleau et al*., 2013], and the NESM consist of alkali basalts to basanites [*Houghton et al*., 1979]. The Virginia-West Virginia Eocene event shares REE signatures with the NESM. The Late Jurassic event was more enriched in REE than the NESM and shares geochemical similarities with the NY kimberlites (elevated Gd/Yb, La/Yb, and Nb/Yb) (Figure 4).

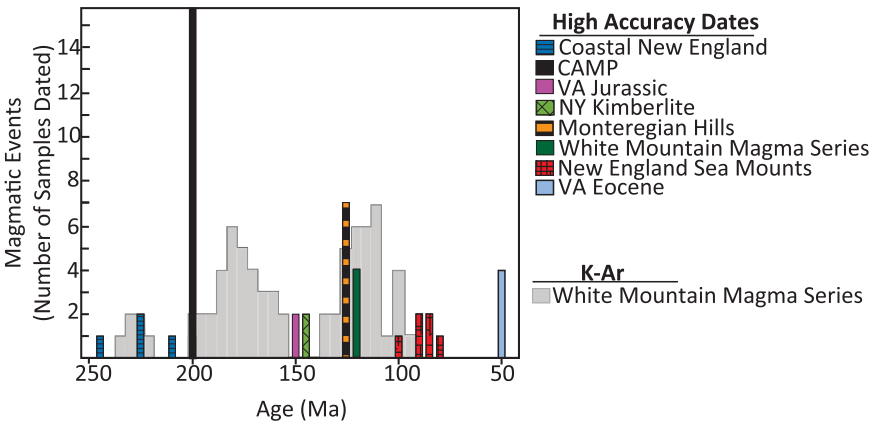

Figure 9. Histogram showing magmatic events that have occurred on the ENAM. Ages come from *Pe-Piper and Reynolds* [2000] and *Ross* [2010] (Coastal New England), *Blackburn et al.* [2013] (CAMP), *Foland and Faul* [1977] and *Hubacher and Foland* [1991] (White Mountain Magma Series for K-Ar and Ar-Ar, respectively), *Heaman and Kjarsgaard* [2000] (NY Kimberlites), *Foland et al.* [1986] (Monteregian Hills), and *Duncan* [1984] (New England Seamounts).

The depletions of Zr and Hf relative to REE of similar compatibility in the upper mantle are often taken as indicators of carbonate metasomatism [*Dupuy et al.*, 1992; *Rudnick et al.*, 1993]. Virginia-West Virginia Eocene volcanics plot, on average, close to what is expected of OIBs, while Virginia-West Virginia Late Jurassic samples have increasingly larger Zr and Hf depletions relative to the REE (low Zr/Sm), pointing toward a source that may have been metasomatized by carbonate-rich fluids (Figure 4e). The Late Jurassic volcanics are also more enriched in Sr (average 1983 ppm) than the Eocene volcanics (average 830 ppm), which can also be an indicator of carbonate metasomatism. The Monteregian Hills and NY kimberlites also have Zr and Hf depletions relative to the REE, and enrichments in Sr, that all trend toward a carbonatite-metasomatized source, consistent with the presence of carbonatites in the Monteregian Hills and the link between kimberlites and carbonate metasomatism.

5.6. Implications for the Postrift Evolution of Passive Margins

Reactivation of a passive margin to a magmatically active margin would require processes that are associated with intraplate volcanism. Mantle plumes, thermochemical anomalies that originate deep within the earth (i.e., the core-mantle boundary) [*Morgan*, 1971; *Wilson*, 1973; *Hofmann and White*, 1982], are one mechanism that can account for postrift magmatism. However, the mantle plume model cannot explain all nontectonic, intraplate magmatism [*Anderson*, 2000; *Anderson and King*, 2014]. Alternative processes in the upper mantle, such as lithospheric delamination [*Ducea and Saleeby*, 1998; *Lustrino*, 2005] and shear-driven upwelling [*Conrad et al.*, 2011] can result in magmatic reactivation of passive margins without a deep mantle source. Lithospheric delamination results from gravitational instabilities in the lower lithosphere causing denser material to pull away and thus allowing warmer, more buoyant asthenospheric material to upwell and melt via decompression. Lithospheric instabilities in rift/postrift settings have been suggested to form due to lateral variations of temperature and density formed during rifting processes [e.g., *Sleep*, 2007]. Such instabilities could allow for local delamination along postrifted margins and associated magmatism [*Meyer and van Wijk*, 2015]. Shear-driven upwelling occurs in the asthenosphere as a result of relative motion of the mantle and a change in lithospheric thickness, such that the asthenosphere will upwell in the region of a lithospheric pocket, or scar during a delamination event [*Conrad et al.*, 2011]. Geodynamic modeling [*Meyer and van Wijk*, 2015] supports the idea that instabilities develop at the edges of rift zones, leading to delamination and associated decompression melting. They showed that the outer margins of rift zones, up to 600 km away from active rifting, could see a thinned mantle lithosphere (up to 25 km of lithospheric thinning), while the upper crust remains unchanged. The extension rate and width of the rift zone do not appear to affect the formation of these instabilities. The development of gravitational instabilities thus triggered delamination and *Meyer and van Wijk* [2015] suggested that the delaminated material undergoes metamorphism, interacting with the surrounding mantle.

Lithospheric delimitation could be an appropriate model for the production of the Late Jurassic volcanics, as proposed by *Meyer and van Wijk* [2015]. While only one sample yielded a melt equilibration temperature,

1351°C is too cold to invoke melting from a mantle plume [e.g., *Lee et al*., 2009]. Based on the depths of melt equilibration for the mafic volcanics at 70 km and the felsic volcanics at 35 km, we suggest that delamination triggered initial melting with upwelling asthenosphere that incorporated lithospheric mantle during fractionation at shallower depths. Melting of other alkaline and volatile-rich volcanics from along the ENAM between ~153 and ~125 Ma, e.g., New York kimberlites and Monteregian Hills alkaline-carbonatite complex, are not the product of lithospheric delamination [e.g., *Roulleau et al*., 2013; *Bailey and Lupulescu*, 2015], but nonetheless sample a similar, volatile-rich, heterogeneous upper mantle as the Late Jurassic volcanics of Virginia-West Virginia.

Mazza et al. [2014] suggested that lithospheric delamination was the cause for the Eocene magmatic pulse by coupling geochemical data with seismic evidence for varying thicknesses of the lithosphere from North Carolina [*Wagner et al*., 2012] and Virginia [*Benoit and Long*, 2009]. Since then, data from the EarthScope and USArray seismic network for the ENAM have confirmed that lithospheric delamination could be a plausible mechanism for Eocene volcanism [*Schmandt and Lin*, 2014; *Liu and Holt*, 2015; *Biryol et al*., 2016; *Porter et al*., 2016]. *Schmandt and Lin* [2014] reported a region of low seismic velocities termed the Central Appalachian anomalous zone, which includes our study area and the presence of a possible lithospheric scar. They suggest that lithospheric delamination could result in the present-day anomaly. *Schmandt and Lin* [2014] also discussed the possibility of the fluids from the Farallon slab affecting the rheology of the upper mantle and thus the low-velocity anomaly. *Biryol et al*. [2016] expanded on these observations with additional data from the Southeastern Suture of the Appalachian Margin Experimental array. They suggest that delamination has been occurring in a piecemeal fashion, which also accounts for the rejuvenated tectonism seen in the ENAM. They suggest that a more recently removed piece of the lithosphere is visible as a fast velocity anomaly within the warmer asthenosphere (see F5 in Figure 10). *Porter et al*. [2016] also agrees that delamination is the most plausible mechanism to explain the observed low-velocity anomaly.

Tomographic cross sections in the region of the Virginia-West Virginia volcanics show a slow-velocity anomaly in the upper mantle (label S2 in Figure 10, tomography from *Biryol et al*. [2016]). The present-day low-velocity anomaly corresponds to the depths of the Eocene melt equilibrium in Figure 10. Eocene mafic melts equilibrated between 2.0 and 3.0 GPa, based on calculations using the *Lee et al*. [2009] geothermobarometer and discussed in detail in *Mazza et al*. [2014]. It remains a possibility that partial melt still exists in this slow-velocity region beneath Virginia, and further geophysical work on the region can help clarify this. The possible ongoing presence of partial melts below Virginia could be due to a simultaneous change in the lithosphere-upper mantle asthenosphere flow due to the timing of the Farallon slab arriving to the ENAM [*Ren et al*., 2007] coupled with the presence of instabilities remnant of rifting. Shear-driven convection [*Ballmer et al*., 2015] cannot be excluded as a possibility for the presence of partial melt and more recent topographic rejuvenation events of the central Appalachians [e.g., *Pazzaglia and Gardner*, 1994; *Rowley et al*., 2013].

6. Conclusions

We conclude that lithospheric instabilities that lead to piecemeal foundering and delamination are probably the trigger that produced the volcanism and rejuvenation seen from Virginia to New England along the ENAM. The complex inheritance of the formation of the Appalachians by multiple collisions resulted in a "passive-aggressive" margin that continued its evolution 200 My after the opening of the Atlantic. We characterized two magmatic events in Virginia-West Virginia following the opening of the Atlantic Ocean basin, with a pulse at ~153 and at ~47 Ma. The Late Jurassic pulse contains highly alkaline magmas, basanites, and trachybasalts to phonolites, with the evolution of these magmas best explained by crystal fractionation at the base of a thinned lithosphere. Sr-Nd-Pb radiogenic isotopes suggest a heterogeneous source, with similar mantle reservoirs also sampled by kimberlites and carbonatites. The late Jurassic magmatic pulses are temporally equivalent with ~147 Ma kimberlites from NY and share isotopic similarities. This suggests that Late Jurassic magmatism was widespread across the ENAM, sampling a uniform upper mantle and was likely caused by tectonic instabilities inherited from rifting of Pangea [*Thomas*, 1977, 2006].

Timing of the Eocene magmatism has been better constrained to 48–47 Ma. The felsic magmas resulted from crystal fractionation of basaltic magmas at shallow depths. Eocene magmas used preexisting shallow crustal features as melt conduits [*Johnson et al*., 2013; *Shada et al*., 2014]. Lithospheric delamination, as

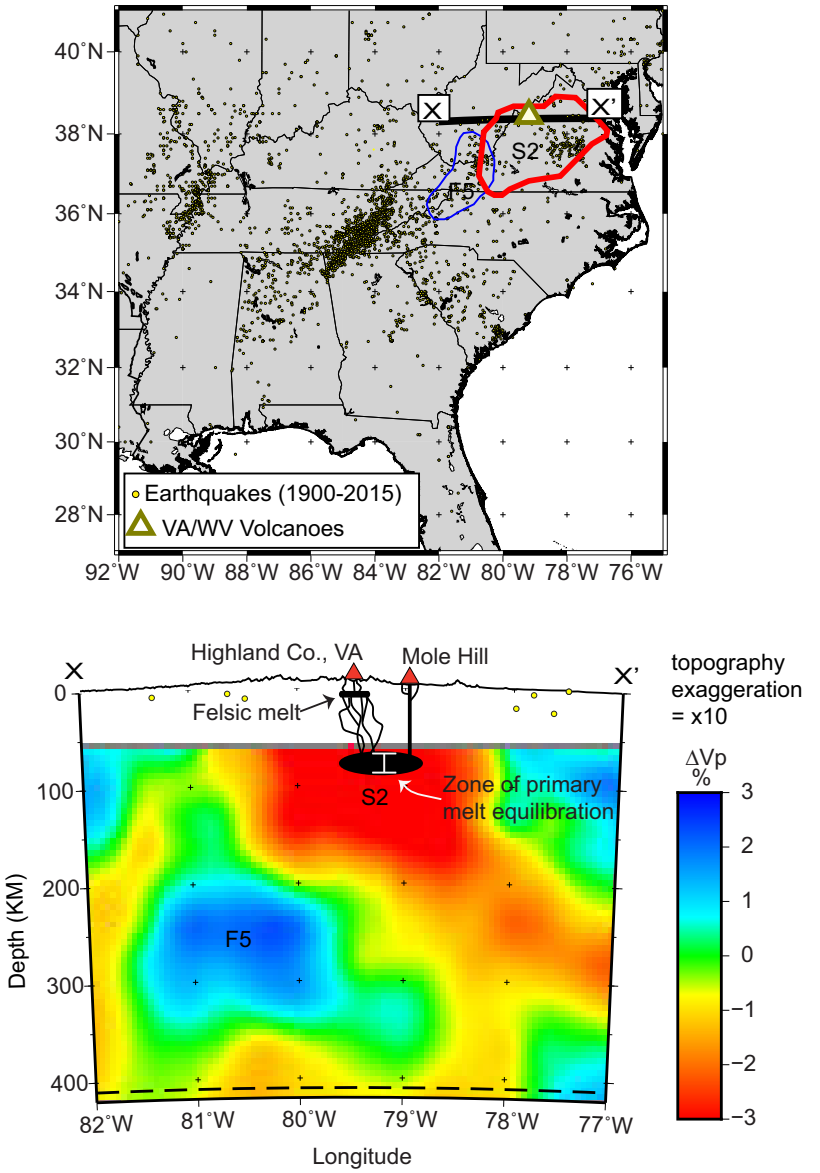

Figure 10. Depths of equilibration and fractional crystallization for Eocene processes, shown in black, coupled with new tomographic results from *Biryol et al.* [2016] from the EarthScope Transportable Array experiment and the Southeastern Suture of the Appalachian Margin experiment across the ENAM. (top) Extent of seismic stations used for tomographic results and (bottom) with X-X' representing the line of section. F5 is a proposed recent piece of delaminated lithosphere, and S2 is the slow velocity anomaly possibly associated with upwelling and the Eocene melting event. Red S2 and Blue F5 shown on the top plot correspond to the regions in the cross section. For full methodology regarding this tomography, see *Biryol et al.* [2016]. Calculated mafic melt equilibrium zones [*Mazza et al.*, 2014] and felsic melt fractional crystallization zone from rhyoliteMELTS.

proposed by *Mazza et al.* [2014] remains the best model for magma production, and has been recently supported by geophysical evidence [e.g., *Schmandt and Lin*, 2014; *Biryol et al.*, 2016].

The ENAM records the evolution of continental rifting, from active supercontinent breakup to the development of a magmatically active margin that retains thermal instabilities up to 50 My after rift initiation. Later rejuvenation associated with the Eocene magmatic pulse and more recent dynamic topography is not connected to the immediate postrift evolution of the margin, but is likely due to ongoing lithospheric delamination.

Acknowledgments
Data for this study can be found in the supporting information section. This project was supported by GeoPrisms-NSF awards EAR-1249412 to E.G. and EAR-1249438 to E.J. We thank JMU undergraduate students B. Soles, G. Brennan, M. Bulas, D. Jones, N. Rossi, A. Wenger, and B. Sacco for sample collection help. This manuscript was improved by discussion with L. Wagner and B. Schmandt. We also thank J. Konter, K. S. Hughes, A. Merschat, and one anonymous reviewer for insightful comments and corrections, and T. Becker for editorial handling of this manuscript.

References

Alexander, E. C., Jr., G. M. Mickelson, and M. A. Lanphere (1978), Mmhb-1: A new 40Ar/39Ar dating standard, in *Short papers of the fourth international conference, geochronology, cosmochronology, and isotope geology 1978*, edited by R. E. Zartman, *U.S. Geol. Surv. Open File Rep. 78-701*, 6–8.

Anderson, D. L. (2000), The thermal state of the upper mantle: No role for mantle plumes, *Geophys. Res. Lett.*, *27*(22), 3623–3626, doi: 10.1029/2000GL011533.

Anderson, D. L., and S. D. King (2014), Driving the Earth machine?, *Science*, *346*(6214), 1184, doi:10.1126/science.1261831.

Araujo, A., R. W. Carlson, J. C. Gaspar, and L. A. Bizzi (2001), Petrology of kamafugites and kimberlites from the Alto Paranaiba alkaline province, Minas Gerais, Brazil, *Contrib. Mineral. Petrol.*, *142*(2), 163–177, doi:10.1007/s004100100280.

Bailey, D. G., and M. V. Lupulescu (2015), Spatial, temporal, mineralogical, and compositional variations in Mesozoic kimberlitic magmatism in New York State, *Lithos*, *212*, 298–310, doi:10.1016/j.lithos.2014.11.022.

Bakun, W., and M. Hopper (2004), Magnitudes and locations of the 1811–1812 New Madrid, Missouri, and the 1886 Charleston, South Carolina, earthquakes, *Bull. Seismol. Soc. Am.*, *94*(1), 64–75, doi:10.1785/0120020122.

Ballmer, M. D., C. P. Conrad, E. I. Smith, and R. Johnsen (2015), Intraplate volcanism at the edges of the Colorado Plateau sustained by a combination of triggered edge-driven convection and shear-driven upwelling, *Geochem. Geophys. Geosyst.*, *16*, 366–379, doi:10.1002/2014GC005641.

Bell, K., and A. Simonetti (1996), Carbonatite magmatism and plume activity: Implications from the Nd, Pb and Sr isotope systematics of Oldoinyo Lengai, *J. Petrol.*, *37*(6), 1321–1339.

Benoit, M., and M. Long (2009), The TEENA experiment: A pilot project to study the structure and dynamics of the eastern US continental margin, *Eos Trans. AGU*, 90(52), Fall Meet. Suppl., Abstract U53A-0053.

Bikerman, M., H. S. Prellwitz, J. Dembosky, A. Simonetti, and K. Bell (1997), New phlogopite K-Ar dates and the age of southwestern Pennsylvania kimberlite dikes, *Northeast. Geol.*, *19*, 302–308.

Biryol, C. B., L. S. Wagner, K. M. Fischer, and R. B. Hawman (2016), Relationship between observed upper mantle structures and recent tectonic activity across the Southeastern United States, *J. Geophys. Res. Solid Earth*, *121*, 3393–3414, doi:10.1002/2015JB012698.

Bizimis, M., V. J. Salters, M. O. Garcia, and M. D. Norman (2013), The composition and distribution of the rejuvenated component across the Hawaiian plume: Hf-Nd-Sr-Pb isotope systematics of Kaula lavas and pyroxenite xenoliths, *Geochem. Geophys. Geosyst.*, *14*, 4458–4478. doi:10.1002/ggge.20250.

Blackburn, T. J., P. E. Olsen, S. A. Bowring, N. M. McLean, D. V. Kent, J. Puffer, G. McHone, E. T. Rasbury, and M. Et-Touhami (2013), Zircon U-Pb geochronology links the end-Triassic extinction with the Central Atlantic Magmatic Province, *Science*, *340*(6135), 941–945, doi: 10.1126/science.1234204.

Bradley, D. C. (2008), Passive margins through earth history, *Earth Sci. Rev.*, *91*(1), 1–26, doi:10.1016/j.earscirev.2008.08.001.

Callegaro, S., A. Marzoli, H. Bertrand, M. Chiaradia, L. Reisberg, C. Meyzen, G. Bellieni, R. E. Weems, and R. Merle (2013), Upper and lower crust recycling in the source of CAMP basaltic dykes from southeastern North America, *Earth Planet. Sci. Lett.*, *376*, 186–199, doi: 10.1016/j.epsl.2013.06.023.

Carrigan, C. W., C. F. Miller, P. D. Fullagar, B. R. Bream, R. D. Hatcher, and C. D. Coath (2003), Ion microprobe age and geochemistry of southern Appalachian basement, with implications for Proterozoic and Paleozoic reconstructions, *Precambrian Res.*, *120*(1), 1–36, doi:10.1016/S0301-9268(02)00113-4.

Carroll, M. R., and J. G. Blank (1997), The solubility of H2O in phonolitic melts, *Am. Mineral.*, *82*(5-6), 549–556, doi:10.2138/am-1997-5-615.

Cebula, G. T., M. J. Kunk, H. H. Mehnert, C. W. Naeseer, J. D. Obradovich, and J. F. Sutter (1986), The Fish Canyon tuff, a potential standard for the 40Ar/39Ar and fission track dating methods, *Terra Cognita*, *6*(2), 1–140.

Chu, R., W. Leng, D. V. Helmberger, and M. Gurnis (2013), Hidden hotspot track beneath the eastern United States, *Nat. Geosci.*, *6*(11), 963–966, doi:10.1038/ngeo1949.

Conrad, C. P., T. A. Bianco, E. I. Smith, and P. Wessel (2011), Patterns of intraplate volcanism controlled by asthenospheric shear, *Nat. Geosci.*, *4*(5), 317–321, doi:10.1038/ngeo1111.

Crough, S. T. (1981), Mesozoic hotspot epeirogeny in eastern North America, *Geology*, *9*(1), 2–6, doi:10.1130/0091-7613(1981)9<2:MHEIEN>2.0.CO;2.

Dalrymple, G. B., E. C. Alexander, M. A. Lanphere, and G. P. Kraker (1981), Irradiation of samples for 40Ar/39Ar dating using the Geological Survey TRIGA reactor, *U.S. Geol. Surv. Prof. Pap.*, *1176*, 1–55.

Davidson, J., S. Turner, H. Handley, C. Macpherson, and A. Dosseto (2007), Amphibole "sponge" in arc crust?, *Geology*, *35*(9), 787–790, doi: 10.1130/G23637A.1.

De Boer, J., J. McHone, J. Puffer, P. Ragland, and D. Whittington (1988), Mesozoic and Cenozoic magmatism, *Geol. North Am.*, *2*, 217–241.

Defant, M. J., and M. S. Drummond (1990), Derivation of some modern arc magmas by melting of young subducted lithosphere, *Nature*, *347*(6294), 662–665, doi:10.1038/347662a0.

Deino, A. L. (2001), *User's Manual for Mass Spec* v. 5.02, 1a, pp. 1–119, Berkeley Geochronol. Cent. Spec. Publ., Berkeley, Calif.

Dennison, J. M., and R. W. Johnson (1971), Tertiary intrusions and associated phenomena near the thirty-eighth parallel fracture zone in Virginia and West Virginia, *Geol. Soc. Am. Bull.*, *82*(2), 501–508, doi: 10.1130/0016-7606(1971)82[501:TIAAPN]2.0.CO;2.

DePaolo, D. J. (1981), Trace element and isotopic effects of combined wallrock assimilation and fractional crystallization, *Earth Planet. Sci. Lett.*, *53*(2), 189–202, doi:10.1016/0012-821X(81)90153-9.

Dicken, C. L., S. W. Nicholson, J. D. Horton, S. A. Kinney, G. Gunther, M. P. Foose, and J. A. Mueller (2005), Preliminary integrated geologic map databases for the United States: Delaware, Maryland, New York, Pennsylvania, and Virginia, *U.S. Geol. Surv. Open File Rep.*, *2331-1258*.

Di Muro, A., B. Villemant, G. Montagnac, B. Scaillet, and B. Reynard (2006), Quantification of water content and speciation in natural silicic glasses (phonolite, dacite, rhyolite) by confocal microRaman spectrometry, *Geochim. Cosmochim. Acta*, *70*(11), 2868–2884, doi:10.1016/j.gca.2006.02.016.

Ducea, M., and J. Saleeby (1998), A case for delamination of the deep batholithic crust beneath the Sierra Nevada, California, *Int. Geol. Rev.*, *40*(1), 78–93, doi:10.1080/00206819809465199.

Duncan, R. A. (1984), Age progressive volcanism in the New England seamounts and the opening of the central Atlantic Ocean, *J. Geophys. Res.*, *89*(B12), 9980–9990.

Dupuy, C., J. Liotard, and J. Dostal (1992), Zr/Hf fractionation in intraplate basaltic rocks: Carbonate metasomatism in the mantle source, *Geochim. Cosmochim. Acta*, *56*(6), 2417–2423, doi:10.1016/0016-7037(92)90198-R.

Ebinger, C., A. Ayele, D. Keir, J. Rowland, G. Yirgu, T. Wright, M. Belachew, and I. Hamling (2010), Length and timescales of rift faulting and magma intrusion: The Afar rifting cycle from 2005 to present, *Annu. Rev. Earth Planet. Sci.*, *38*, 439–466, doi:10.1146/annurev-earth-040809-152333.

Eby, G. N. (1984), Geochronology of the Monteregian Hills alkaline igneous province, Quebec, *Geology*, *12*(8), 468–470, doi:10.1130/0091-7613(1984)12 < 468:GOTMHA>2.0.CO;2.

Eby, G. N. (1985), Age relations, chemistry, and petrogenesis of mafic alkaline dikes from the Monteregian Hills and younger White Mountain igneous provinces, *Can. J. Earth Sci.*, *22*(8), 1103–1111, doi:10.1139/e85-112.

Faill, R. T. (1998), A geologic history of the north-central Appalachians; Part 3, The Alleghany Orogeny, *Am. J. Sci.*, *298*(2), 131–179, doi:10.2475/ajs.298.2.131.

Foland, K., and H. Faul (1977), Ages of the White Mountain intrusives; New Hampshire, Vermont, and Maine, USA, *Am. J. Sci.*, *277*(7), 888–904, doi:10.2475/ajs.277.7.888.

Foland, K., L. A. Gilbert, C. A. Sebring, and C. Jiang-Feng (1986), 40Ar/39Ar ages for plutons of the Monteregian Hills, Quebec: Evidence for a single episode of Cretaceous magmatism, *Geol. Soc. Am. Bull.*, *97*(8), 966–974, doi:10.1130/0016-7606(1986)97.

Fullagar, P., and M. L. Bottino (1969), Tertiary felsite intrusions in the Valley and Ridge province, Virginia, *Geol. Soc. Am. Bull.*, *80*(9), 1853–1858, doi: 10.1130/0016-7606(1969)80[1853:TFIITV]2.0.CO;2.

Gallen, S. F., K. W. Wegmann, and D. Bohnenstiehl (2013), Miocene rejuvenation of topographic relief in the southern Appalachians, *GSA Today*, *23*(2), 4–10, doi:10.1130/GSATG163A.1.

Gazel, E., T. Plank, D. W. Forsyth, C. Bendersky, C. T. A. Lee, and E. H. Hauri (2012), Lithosphere versus asthenosphere mantle sources at the Big Pine Volcanic Field, California, *Geochem. Geophys. Geosyst.*, *13*, Q0AK06, doi:10.1029/2012GC004060.

Gualda, G. A., M. S. Ghiorso, R. V. Lemons, and T. L. Carley (2012), Rhyolite-MELTS: A modified calibration of MELTS optimized for silica-rich, fluid-bearing magmatic systems, *J. Petrol.*, *53*(5), 875–890, doi:10.1093/petrology/egr080.

Hatcher, R. D. (2002), Alleghanian (Appalachian) orogeny, a product of zipper tectonics: Rotational transpressive continent-continent collision and closing of ancient oceans along irregular margins, *Geol. Soc. Am. Spec. Pap.*, *364*, 199–208.

Hatcher, R. D. (2010), The Appalachian orogen: A brief summary, *Geol. Soc. Am. Mem.*, *206*, 1–19. doi:10.1130/2010.1206(01).

Haugerud, R. A., and M. J. Kunk (1988), ArAr*, a computer program for reduction of 40Ar-39Ar data, *U.S. Geol. Surv. Open File Rep.*, 88–261, 67 pp.

He, Z., F. Huang, H. Yu, Y. Xiao, F. Wang, Q. Li, Y. Xia, and X. Zhang (2015), A flux-free fusion technique for rapid determination of major and trace elements in silicate rocks by LA-ICP-MS, *Geostand. Geoanal. Res.*, *40*(1), 5–21, doi:10.1111/j.1751-908X.2015.00352.x.

Heaman, L., and B. Kjarsgaard (2000), Timing of eastern North American kimberlite magmatism: Continental extension of the Great Meteor hotspot track?, *Earth Planet. Sci. Lett.*, *178*(3), 253–268, doi:10.1016/S0012-821X(00)00079-0.

Hofmann, A. W., and W. M. White (1982), Mantle plumes from ancient oceanic crust, *Earth Planet. Sci. Lett.*, *57*(2), 421–436, doi:10.1016/0012-821X(82)90161-3.

Hofmann, A. W., K. Jochum, M. Seufert, and W. White (1986), Nb and Pb in oceanic basalts: New constraints on mantle evolution, *Earth Planet. Sci. Lett.*, *79*(1-2), 33–45, doi:10.1016/0012-821X(86)90038-5.

Holm, P. M., J. R. Wilson, B. P. Christensen, L. Hansen, S. L. Hansen, K. M. Hein, A. K. Mortensen, R. Pedersen, S. Plesner, and M. K. Runge (2005), Sampling the Cape Verde mantle plume: Evolution of melt compositions on Santo Antão, Cape Verde Islands, *J. Petrol.*, *47*(1), 145–189, doi:10.1093/petrology/egi071.

Horton, J. W., M. C. Chapman, and R. A. Green (2015), The 2011 Mineral, Virginia, earthquake, and its significance for seismic hazards in eastern North America—Overview and synthesis, *Geol. Soc. Am. Spec. Pap.*, *509*, 1–25, doi:10.1130/2015.2509(01).

Houghton, R., J. Thomas, R. Diecchio, and A. Tagliacozzo (1979), Radiometric ages of basalts from DSDP Leg 43: Sites 382 and 385 (New England seamounts), 384 (J Anomaly), 386 and 387 (central and western Bermuda Rise), edited by B. C. Tucholke and P. R. Vogt, *Initial Rep. Deep Sea Drill. Proj.*, 43, 721–738.

Hubacher, F., and K. Foland (1991), 40Ar/39Ar ages for Cretaceous intrusions of the White Mountain magma series, northern New England, and their tectonic implications, *Geol. Soc. Am. Abstr. Programs*, *23*(1), 47.

Izzeldin, A. (1987), Seismic, gravity and magnetic surveys in the central part of the Red Sea: Their interpretation and implications for the structure and evolution of the Red Sea, *Tectonophysics*, *143*(4), 269–306, doi:10.1016/0040-1951(87)90214-9.

Jansa, L. F., and G. Pe-Piper (1988), Middle Jurassic to Early Cretaceous igneous rocks along eastern North American continental margin, *AAPG Bull.*, *72*(3), 347–366.

Johnson, E. A., Z. A. Kiracofe, J. T. Haynes, and K. Nashimoto (2013). The origin of sandstone xenoliths in the Mole Hill Basalt, Rockingham County, Virginia; Implications for magma ascent and crustal structure in the Western Shenandoah Valley, *Southeast. Geol.*, *49*(3), 95–118.

Johnson, K. T. (1998), Experimental determination of partition coefficients for rare earth and high-field-strength elements between clinopyroxene, garnet, and basaltic melt at high pressures, *Contrib. Mineral. Petrol.*, *133*(1-2), 60–68, doi:10.1007/s004100050437.

Johnson, R. W., C. Milton, and J. M. Dennison (1971), Field trip to the igneous rocks of Augusta, Rockingham, Highland, and Bath counties, Virginia, *Va. Div. Mineral Resour.*, *16*, 1–68.

Khanna, T. C., M. Bizimis, G. M. Yogodzinski, and S. Mallick (2014), Hafnium–neodymium isotope systematics of the 2.7 Ga Gadwal greenstone terrane, Eastern Dharwar craton, India: Implications for the evolution of the Archean depleted mantle, *Geochim. Cosmochim. Acta*, *127*, 10–24, doi:10.1016/j.gca.2013.11.024.

Kelley, K. A., T. Plank, J. Ludden, and H. Staudigel (2003), Composition of altered oceanic crust at ODP Sites 801 and 1149, *Geochem. Geophys. Geosyst.*, *4*(6), 8910, doi:10.1029/2002GC000435.

Klaudius, J., and J. Keller (2006), Peralkaline silicate lavas at Oldoinyo Lengai, Tanzania, *Lithos*, *91*(1), 173–190, doi:10.1016/j.lithos.2006.03.017.

Klitgord, K. D., D. R. Hutchinson, and H. Schouten (1988), US Atlantic continental margin; structural and tectonic framework, *Geol. North Am.*, *2*, 19–55.

Korostelev, F., S. Leroy, D. Keir, C. Weemstra, L. Boschi, I. Molinari, A. Ahmed, G. W. Stuart, F. Rolandone, and K. Khanbari (2016), Magmatism at continental passive margins inferred from Ambient-Noise Phase-velocity in the Gulf of Aden, *Terra Nova*, *28*(1), 19–26, doi:10.1111/ter.12182.

Kunk, M. J., and R. McAleer (2011), 40Ar/39Ar Age-spectrum data for hornblende, biotite, white mica, and K-feldspar samples from metamorphic rocks in the Great Smokey Mountains of North Carolina and Tennessee, *U.S. Geol. Surv. Open File Rep.*, *2011-1250*, 1–56.

Kunk, M. J., J. F. Sutter, and C. W. Naeser (1985), High-precision 40Ar/39Ar Ages of Sanidine, Biotite, Hornblende, and Plagioclase from the Fish Canyon Tuff, San Juan Volcanic Field, South-central Colorado, *Geol. Soc. Am. Abstr. Programs*, *17*, 636.

Lee, C.-T. A., P. Luffi, T. Plank, H. Dalton, and W. P. Leeman (2009), Constraints on the depths and temperatures of basaltic magma generation on Earth and other terrestrial planets using new thermobarometers for mafic magmas, *Earth Planet. Sci. Lett.*, *279*(1), 20–33, doi:10.1016/j.epsl.2008.12.020.

LeMasurier, W. E., S. H. Choi, Y. Kawachi, S. B. Mukasa, and N. Rogers (2011), Evolution of pantellerite-trachyte-phonolite volcanoes by fractional crystallization of basanite magma in a continental rift setting, Marie Byrd Land, Antarctica, *Contrib. Mineral. Petrol.*, *162*(6), 1175–1199, doi:10.1007/s00410-011-0646-z.

Le Roex, A., R. Cliff, and B. Adair (1990), Tristan da Cunha, South Atlantic: Geochemistry and petrogenesis of a basanite-phonolite lava series, *J. Petrol.*, *31*(4), 779–812, doi:10.1093/petrology/31.4.779.

Liu, T.-C., and D. Presnall (2000), Liquidus phase relations in the system CaO–MgO–Al2O3–SiO2 at 2·0 GPa: Applications to basalt fractionation, eclogites, and igneous sapphirine, *J. Petrol.*, *41*(1), 3–20, doi:10.1093/petrology/41.1.3.

Liu, Y., and W. E. Holt (2015), Wave gradiometry and its link with Helmholtz equation solutions applied to USArray in the eastern US, *J. Geophys. Res. Solid Earth*, *120*, 5717–5746, doi:10.1002/2015JB011982.

Lustrino, M. (2005), How the delamination and detachment of lower crust can influence basaltic magmatism, *Earth Sci. Rev.*, *72*(1), 21–38, doi:10.1016/j.earscirev.2005.03.004.

Mana, S., T. Furman, M. Carr, G. Mollel, R. Mortlock, M. Feigenson, B. Turrin, and C. Swisher (2012), Geochronology and geochemistry of the Essimingor volcano: Melting of metasomatized lithospheric mantle beneath the North Tanzanian Divergence zone (East African Rift), *Lithos*, *155*, 310–325, doi:10.1016/j.lithos.2012.09.009.

Martin, H. (1999), Adakitic magmas: Modern analogues of Archaean granitoids, *Lithos*, *46*(3), 411–429, doi:10.1016/S0024-4937(98)00076-0.

Marzoli, A., F. Jourdan, J. H. Puffer, T. Cuppone, L. H. Tanner, R. E. Weems, H. Bertrand, S. Cirilli, G. Bellieni, and A. De Min (2011), Timing and duration of the Central Atlantic magmatic province in the Newark and Culpeper basins, eastern USA, *Lithos*, *122*(3), 175–188, doi:10.1016/j.lithos.2010.12.013.

Maury, R. C., F. G. Sajona, M. Pubellier, H. Bellon, and M. J. Defant (1996), Fusion de la croute oceanique dans les zones de subduction/collision recentes; l'exemple de Mindanao (Philippines), *Bull. Soc. Géol. France*, *167*(5), 579–595.

Mazza, S. E., E. Gazel, E. A. Johnson, M. J. Kunk, R. McAleer, J. A. Spotila, M. Bizimis, and D. S. Coleman (2014), Volcanoes of the passive margin: The youngest magmatic event in eastern North America, *Geology*, *42*(6), 483–486, doi:10.1130/G35407.1.

McDougall, I., and T. M. Harrison (1999), *Geochronology and Thermochronology by the 40Ar/39Ar Method*, Oxford University Press, New York.

McDonough, W. F., and S.-S. Sun (1995), The composition of the Earth, *Chem. Geol.*, *120*(3), 223–253, doi:10.1016/0009-2541(94)00140-4.

McHone, J. G. (1996), Constraints on the mantle plume model for Mesozoic alkaline intrusions in northeastern North America, *Can. Mineral.*, *34*, 325–334.

McHone, J. G., and J. R. Butler (1984), Mesozoic igneous provinces of New England and the opening of the North Atlantic Ocean, *Geol. Soc. Am. Bull.*, *95*(7), 757–765, doi:10.1130/0016-7606(1984)95.

McKenzie, D., and R. O'Nions (1991), Partial melt distributions from inversion of rare earth element concentrations, *J. Petrol.*, *32*(5), 1021–1091, doi:10.1093/petrology/32.5.1021.

McKeon, R. E., P. K. Zeitler, F. J. Pazzaglia, B. D. Idleman, and E. Enkelmann (2014), Decay of an old orogen: Inferences about Appalachian landscape evolution from low-temperature thermochronology, *Geol. Soc. Am. Bull.*, *126*(1–2), 31–46, doi:10.1130/B30808.1.

Meyer, R., and J. van Wijk (2015), Post-breakup lithosphere recycling below the US East Coast: Evidence from adakitic rocks, *Geol. Soc. Am. Spec. Pap.*, *514*, 65–85, doi:10.1130/2015.2514(06).

Miller, S. R., P. B. Sak, E. Kirby, and P. R. Bierman (2013), Neogene rejuvenation of central Appalachian topography: Evidence for differential rock uplift from stream profiles and erosion rates, *Earth Planet. Sci. Lett.*, *369*, 1–12, doi:10.1016/j.epsl.2013.04.007.

Morgan, W. J. (1971), Convection plumes in the lower mantle, *Nature*, *230*, 42–43, doi:10.1038/230042a0.

Nomade, S., K. Knight, E. Beutel, P. Renne, C. Verati, G. Féraud, A. Marzoli, N. Youbi, and H. Bertrand (2007), Chronology of the Central Atlantic Magmatic Province: Implications for the Central Atlantic rifting processes and the Triassic–Jurassic biotic crisis, *Palaeogeogr. Palaeoclimatol. Palaeoecol.*, *244*(1), 326–344, doi:10.1016/j.palaeo.2006.06.034.

Pallister, J. S., W. A. McCausland, S. Jónsson, Z. Lu, H. M. Zahran, S. El Hadidy, A. Aburukbah, I. C. Stewart, P. R. Lundgren, and R. A. White (2010), Broad accommodation of rift-related extension recorded by dyke intrusion in Saudi Arabia, *Nat. Geosci.*, *3*(10), 705–712, doi:10.1038/ngeo966.

Panter, K. S., P. R. Kyle, and J. L. Smellie (1997), Petrogenesis of a phonolite–trachyte succession at Mount Sidley, Marie Byrd Land, Antarctica, *J. Petrol.*, *38*(9), 1225–1253, doi:10.1093/petroj/38.9.1225.

Pazzaglia, F. J., and M. T. Brandon (1996), Macrogeomorphic evolution of the post-Triassic Appalachian mountains determined by deconvolution of the offshore basin sedimentary record, *Basin Res.*, *8*(3), 255–278, doi:10.1046/j.1365-2117.1996.00274.x.

Pazzaglia, F. J., and T. W. Gardner (1994), Late Cenozoic flexural deformation of the middle US Atlantic passive margin, *J. Geophys. Res.*, *99*(B6), 12,143–12,157, doi:10.1029/93JB03130.

Pearce, J. A. (2008), Geochemical fingerprinting of oceanic basalts with applications to ophiolite classification and the search for Archean oceanic crust, *Lithos*, *100*(1), 14–48, doi:10.1016/j.lithos.2007.06.016.

Pelleter, A.-A., M. Caroff, C. Cordier, P. Bachelery, P. Nehlig, D. Debeuf, and N. Arnaud (2014), Melilite-bearing lavas in Mayotte (France): An insight into the mantle source below the Comores, *Lithos*, *208*, 281–297, doi:10.1016/j.lithos.2014.09.012.

Pe-Piper, G., and P. H. Reynolds (2000), Early Mesozoic alkaline mafic dykes, southwestern Nova Scotia, Canada, and their bearing on Triassic–Jurassic magmatism, *Can. Mineral.*, *38*(1), 217–232, doi:10.2113/gscanmin.38.1.217.

Pettingill, H. S., A. Sinha, and M. Tatsumoto (1984), Age and origin of anorthosites, charnockites, and granulites in the central Virginia Blue Ridge: Nd and Sr isotopic evidence, *Contrib. Mineral. Petrol.*, *85*(3), 279–291, doi:10.1007/BF00378106.

Porter, R., Y. Liu, and W. E. Holt (2016), Lithospheric records of orogeny within the continental US, *Geophys. Res. Lett.*, *43*, 144–153, doi:10.1002/2015GL066950.

Prince, P. S., and J. A. Spotila (2013), Evidence of transient topographic disequilibrium in a landward passive margin river system: Knickpoints and paleo-landscapes of the New River basin, southern Appalachians, *Earth Surf. Processes Landforms*, *38*(14), 1685–1699, doi:10.1002/esp.3406.

Puffer, J. (2001), Contrasting high field strength element contents of continental flood basalts from plume versus reactivated-arc sources, *Geology*, *29*(8), 675–678, doi:10.1130/0091-7613(2001)029.

Puffer, J. H. (2003), A Reactivated Back-Arc Source for CAMP Magma, in *The Central Atlantic Magmatic Province: Insights from Fragments of Pangea*, edited by W. Hames et al., pp. 151–162, AGU, Washington, D. C., doi:10.1029/136GM08.

Ren, Y., E. Stutzmann, R. D. van Der Hilst, and J. Besse (2007), Understanding seismic heterogeneities in the lower mantle beneath the Americas from seismic tomography and plate tectonic history, *J. Geophys. Res.*, *112*, B01302, doi:10.1029/2005JB004154.

Rollinson, H. (1993), *Using Geochemical Data: Evaluation, Interpretation, Presentation*, p. 52–61, Longman, New York.

Ross, M. E. (2010), An Early Triassic 40Ar/39Ar age for a camptonite dyke in Cambridge, Massachusetts, USA, *Atlant. Geol.*, *46*(1), 127–135, doi:10.4138/atlgeol.2010.007.

Roulleau, E., R. Stevenson, and A. Polat (2013), Geochemical and isotopic (Nd–Sr–Hf–Pb) evidence for a lithospheric mantle source in the formation of the alkaline Monteregian Province (Quebec), *Can. J. Earth Sci.*, *50*(6), 650–666, doi:10.1139/cjes-2012-0145.
Rowley, D. B., A. M. Forte, R. Moucha, J. X. Mitrovica, N. A. Simmons, and S. P. Grand (2013), Dynamic topography change of the eastern United States since 3 million years ago, *Science*, *340*(6140), 1560–1563, doi:10.1126/science.1229180.
Rudnick, R. L., W. F. McDonough, and B. W. Chappell (1993), Carbonatite metasomatism in the northern Tanzanian mantle: Petrographic and geochemical characteristics, *Earth Planet. Sci. Lett.*, *114*(4), 463–475, doi:10.1016/0012-821X(93)90076-L.
Sacco, B., E. A. Johnson, and H. E. Belkin (2011), Depth and temperature of the mantle beneath Mole Hill, an Eocene basalt near Harrisonburg, VA, *Geol. Soc. Am. Abstr. Programs*, *45*(5), 115.
Sahota, G., P. Styles, and K. Gerdes (1995), Evolution of the Gulf of Aden and implications for the development of the Red Sea, in *Rift Sedimentation and Tectonics in the Red Sea-Gulf of Aden Region*, pp. 1–56, University of Sanāa, Yemen.
Salters, V. J., J. E. Longhi, and M. Bizimis (2002), Near mantle solidus trace element partitioning at pressures up to 3.4 GPa, *Geochem. Geophys. Geosyst.*, *3*(7), doi:10.1029/2001GC000148.
Samson, S. D. (1996), 40Ar/39Ar and Nd-Sr isotopic characteristics of mid-Ordovician North American K-Bentonites: A test of early Paleozoic Laurentia-Gondwana interactions, *Tectonics*, *15*(5), 1084–1092, doi:10.1029/96TC00829.
Samson, S. D., D. G. Coler, and J. A. Speer (1995), Geochemical and Nd Sr Pb isotopic composition of Alleghenian granites of the southern Appalachians: Origin, tectonic setting, and source characterization, *Earth Planet. Sci. Lett.*, *134*(3), 359–376, doi:10.1016/0012-821X(95)00124-U.
Schmandt, B., and F. C. Lin (2014), P and S wave tomography of the mantle beneath the United States, *Geophys. Res. Lett.*, *41*, 6342–6349, doi:10.1002/2014GL061231.
Shada, J. M., E. A. Johnson, S. Whitmeyer, and B. Cohick (2014), Structural controls on the method of Eocene magmatic intrusion in Blue Grass Valley, Highland County, Virginia, *Geol. Soc. Am. Abstr. Programs*, *46*(3).
Siebel, W., R. Becchio, F. Volker, M. Hansen, J. Viramonte, R. Trumbull, G. Haase, and M. Zimmer (2000), Trindade and Martín Vaz Islands, South Atlantic: Isotopic (Sr, Nd, Pb) and trace element constraints on plume related magmatism, *J. S. Am. Earth Sci.*, *13*(1), 79–103, doi:10.1016/S0895-9811(00)00015-8.
Sinha, A., J. Hogan, and J. Parks (1996), Lead isotope mapping of crustal reservoirs within the Grenville Superterrane: I. Central and Southern Appalachians, in Earth Processes: Reading the Isotopic Code, *American Geophysical Union Geophysical Monographs, 95*, 293–305.
Sleep, N. H. (2007), Edge-modulated stagnant-lid convection and volcanic passive margins, *Geochem. Geophys. Geosyst.*, *8*, Q12004, doi:10.1029/2007GC001672.
Streckeisen, A. (1979), Classification and nomenclature of volcanic rocks, lamprophyres, carbonatites, and melilitic rocks: Recommendations and suggestions of the IUGS Subcommission on the Systematics of Igneous Rocks, *Geology*, *7*(7), 331–335, doi:10.1130/0091-7613(1979)7.
Soles, B., G. Brennan, E. Johnson, S. Mazza, and E. Gazel (2014), Variable water concentrations in the asthenospheric and lithospheric mantle underneath the Eastern United States, Abstract ED31F-3491 presented at 2014 AGU Fall Meeting, AGU, San Francisco, Calif.
Southworth, C. S., K. J. Gray, and J. F. Sutter (1993), Middle Eocene intrusive igneous rocks of the central Appalachian Valley and Ridge province-setting, chemistry, and implications for crustal structure, *U.S. Geol. Surv. Bull.*, *1839*, 1–24.
Stracke, A., A. W. Hofmann, and S. R. Hart (2005), FOZO, HIMU, and the rest of the mantle zoo, *Geochem. Geophys. Geosyst.*, *6*, Q05007, doi:10.1029/2004GC000824.
Thomas, W. A. (1977), Evolution of Appalachian-Ouachita salients and recesses from reentrants and promontories in the continental margin, *Am. J. Sci.*, *277*(10), 1233–1278, doi:10.2475/ajs.277.10.1233.
Thomas, W. A. (2006), Tectonic inheritance at a continental margin, *GSA Today*, *16*(2), 4–11, doi:10.1130/1052-5173(2006)016<4:TIAACM>2.0.CO;2.
Tollo, R. P., J. N. Aleinikoff, M. J. Bartholomew, and D. W. Rankin (2004), Neoproterozoic A-type granitoids of the central and southern Appalachians: Intraplate magmatism associated with episodic rifting of the Rodinian supercontinent, *Precambrian Res.*, *128*(1), 3–38, doi:10.1785/0120020122.
Tso, J. L., and J. D. Surber (2006), Eocene igneous rocks near Monterey, Virginia: A field study, *Va. Minerals*, *49*(3-4), 9–24.
Tso, J. L., R. R. McDowell, K. L. Avary, D. L. Matchen, and G. P. Wilkes (2004), Middle Eocene igneous rocks in the Valley and Ridge of Virginia and West Virginia, *U.S. Geol. Surv. Circ.*, *1624*, 137–157.
Tuff, J., E. Takahashi, and S. Gibson (2005), Experimental constraints on the role of garnet pyroxenite in the genesis of high-Fe mantle plume derived melts, *J. Petrol.*, *46*(10), 2023–2058, doi:10.1093/petrology/egi046.
Vogt, P. R. (1991), Bermuda and Appalachian-Labrador rises: Common non-hotspot processes?, *Geology*, *19*(1), 41–44, doi:10.1130/0091-7613(1991)019<0041:BAALRC>2.3.CO;2.
Wagner, L. S., K. Stewart, and K. Metcalf (2012), Crustal-scale shortening structures beneath the Blue Ridge Mountains, North Carolina, USA, *Lithosphere*, *4*(3), 242–256, doi:10.1130/L184.1.
Weaver, B. L. (1990), Geochemistry of highly-undersaturated ocean island basalt suites from the South Atlantic Ocean: Fernando de Noronha and Trindade islands, *Contrib. Mineral. Petrol.*, *105*(5), 502–515, doi:10.1007/BF00302491.
Weis, D., F. Frey, H. Leyrit, and I. Gautier (1993), Kerguelen Archipelago revisited: Geochemical and isotopic study of the Southeast Province lavas, *Earth Planet. Sci. Lett.*, *118*(1), 101–119, doi:10.1016/0012-821X(93)90162-3.
Whalen, L., E. Gazel, C. Vidito, J. Puffer, M. Bizimis, W. Henika, and M. J. Caddick (2015), Supercontinental inheritance and its influence on supercontinental breakup: The Central Atlantic Magmatic Province and the breakup of Pangea, *Geochem. Geophys. Geosyst.*, *16*, 3532–3554, doi:10.1002/2015GC005885.
White, W. M., F. Albarède, and P. Télouk (2000), High-precision analysis of Pb isotope ratios by multi-collector ICP-MS, *Chem. Geol.*, *167*(3), 257–270, doi:10.1016/S0009-2541(99)00182-5.
Wiesmaier, S., V. R. Troll, J. C. Carracedo, R. M. Ellam, I. Bindeman, and J. A. Wolff (2012), Bimodality of lavas in the Teide–Pico Viejo succession in Tenerife—the role of crustal melting in the origin of recent phonolites, *J. Petrol.*, *53*(12), 2465–2495, doi:10.1093/petrology/egs056.
Willbold, M., and K. P. Jochum (2005), Multi-element isotope dilution sector field ICP-MS: A precise technique for the analysis of geological materials and its application to geological reference materials, *Geostand. Geoanal. Res.*, *29*(1), 63–82, doi:10.1111/j.1751-908X.2005.tb00656.x.
Wilson, J. T. (1973), Mantle plumes and plate motions, *Tectonophysics*, *19*(2), 149–164, doi:10.1016/0040-1951(73)90037-1.
Wilson, M. (1997), Thermal evolution of the Central Atlantic passive margins: Continental break-up above a Mesozoic super-plume, *J. Geol. Soc.*, *154*(3), 491–495, doi:10.1144/gsjgs.154.3.0491.
Xu, J.-F., R. Shinjo, M. J. Defant, Q. Wang, and R. P. Rapp (2002), Origin of Mesozoic adakitic intrusive rocks in the Ningzhen area of east China: Partial melting of delaminated lower continental crust?, *Geology*, *30*(12), 1111–1114, doi:10.1130/0091-7613(2002)030.
Zartman, R., M. Brock, A. Heyl, and H. Thomas (1967), K-Ar and Rb-Sr ages of some alkalic intrusive rocks from central and eastern United States, *Am. J. Sci.*, *265*(10), 848–870, doi:10.2475/ajs.265.10.848.
Zindler, A., and S. Hart (1986), Chemical geodynamics, *Annu. Rev. Earth Planet. Sci.*, *14*, 493–571, doi:10.1146/annurev.ea.14.050186.002425.